

Constraints on the Dark Matter Particle Mass from the Number of Milky Way Satellites

Emil Polisensky^{1,2} and Massimo Ricotti²

¹*Naval Research Laboratory, Washington, D.C. 20375, USA*

²*Department of Astronomy, University of Maryland, College Park, Maryland 20745, USA**

(Dated: November 6, 2018)

We have conducted N -body simulations of the growth of Milky Way-sized halos in cold and warm dark matter cosmologies. The number of dark matter satellites in our simulated Milky Ways decreases with decreasing mass of the dark matter particle. Assuming that the number of dark matter satellites exceeds or equals the number of observed satellites of the Milky Way we derive lower limits on the dark matter particle mass. We find with 95% confidence $m_s > 13.3$ keV for a sterile neutrino produced by the Dodelson and Widrow mechanism, $m_s > 8.9$ keV for the Shi and Fuller mechanism, $m_s > 3.0$ keV for the Higgs decay mechanism, and $m_{WDM} > 2.3$ keV for a thermal dark matter particle. The recent discovery of many new dark matter dominated satellites of the Milky Way in the Sloan Digital Sky Survey allows us to set lower limits comparable to constraints from the complementary methods of Lyman- α forest modeling and X-ray observations of the unresolved cosmic X-ray background and of dark matter halos from dwarf galaxy to cluster scales. Future surveys like LSST, DES, PanSTARRS, and SkyMapper have the potential to discover many more satellites and further improve constraints on the dark matter particle mass.

I. INTRODUCTION

Cold dark matter (CDM) is extremely successful at describing the large scale features of matter distribution in the Universe but has problems on small scales. Below the Mpc scale CDM predicts numbers of satellite galaxies for Milky Way-sized halos about an order of magnitude in excess of the number observed. This is the ‘missing satellites’ problem [1, 2]. One proposed solution is that, due to feedback mechanisms, some dark matter satellites do not form stars and are nonluminous dark halos [3–7]. Another solution is the power spectrum of density fluctuations may be truncated which may arise if the dark matter is ‘warm’ (particle mass ~ 1 keV) instead of ‘cold’ (particle mass ~ 1 GeV). Warm dark matter (WDM) particles decouple from the other particle species in the early Universe with relativistic velocities and only become nonrelativistic when about a Galactic mass ($\sim 10^{12} M_\odot$) is within the horizon. Streaming motions while the particles are still relativistic can erase density fluctuations on sub-Galactic scales and reduce the number of satellites. WDM models have been studied by a number of authors [8–14] in relation to the missing satellites problem and other issues with CDM such as the apparent density cores in spiral and dwarf galaxies [15–23].

N -body simulations of WDM cosmologies are complicated by numerical artifacts produced by the discrete sampling of the gravitational potential with a finite number of particles (see [24] for a review). Matter perturbations collapse and form filaments with nonphysical halos separated by a distance equal to the mean particle spacing (see Fig. 1) [24, 25]. These halos are numerical

artifacts. The ability of these halos to survive disruption as they accrete from filaments onto Milky Way-sized halos has not been studied and they may contaminate the satellite abundances and distributions in WDM simulations.

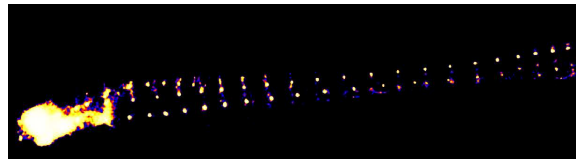


FIG. 1. Nonphysical halos formed along a filament and accreting onto a larger halo at $z = 1$ in a WDM simulation ($m_{WDM} = 1$ keV). These halos are numerical artifacts.

In the past few years, 16 new dwarf spheroidal galaxies have been discovered in the Sloan Digital Sky Survey (SDSS) [26] (see Table 3 and references therein). After correcting for completeness the estimated number of Milky Way (MW) satellites is > 60 (see Sec. III C). These new dwarfs have low luminosities, low surface brightnesses, and most appear to be dark matter dominated. Since the number of dark matter halos must be greater than or equal to the number of observed satellites, the new data from the SDSS may provide improved limits on the mass of the dark matter particle independent of complementary techniques.

Motivated by the recent increase in the number of observed Milky Way satellites, we have performed new simulations of the growth of Milky Way-like galaxies in CDM and WDM cosmologies for a variety of WDM particle masses. Our goal is to constrain the dark matter particle mass by comparing the number of satellite halos in the simulated Milky Ways to the observed number of luminous satellites for the actual Milky Way. Macciò and Fontanot [14] combined N -body simulations with semi-

* emilp@astro.umd.edu

analytic models of galaxy formation to compare the simulated and observed Milky Way satellite luminosity functions for CDM and WDM cosmologies. In this work, we do not make any assumptions on how we populate dark matter halos with luminous galaxies. We simply impose that the number of observed satellites is less than or equal to the number of dark matter halos for a range of Galactocentric radii. This guarantees a robust lower limit on the dark matter particle mass.

II. SIMULATIONS

All our simulations were conducted with the N -body cosmological simulation code GADGET-2 [27] assuming dark matter only. We adopted values for cosmological parameters from the third year release of the WMAP mission [28], $(\Omega_m, \Omega_\Lambda, h, \sigma_8, n_s) = (0.238, 0.762, 0.73, 0.751, 0.951)$ to facilitate comparison with the Via Lactea II simulation [29]. For each simulation set we produced a single realization of the density field in the same periodic, comoving volume but varied the power spectrum of fluctuations appropriate for CDM and WDM cosmologies. Our initial conditions were generated on a cubic lattice using the GRAFIC2 software package [30]. The power spectra for CDM and WDM are given by

$$P_{CDM}(k) \propto k^{n_s} T_{CDM}^2, \quad (1)$$

$$P_{WDM}(k) = P_{CDM} T_{WDM}^2, \quad (2)$$

respectively, with the normalization of P_{CDM} determined by σ_8 . For our first two sets of simulations (*set A* and *B* described below) we used the transfer function for CDM adiabatic fluctuations given by Bardeen et al. (BBKS) [31]:

$$T_{CDM}(k) = \frac{\ln(1 + 2.34q)}{2.34q} [1 + 3.89q + (16.1q)^2 + (5.46q)^3 + (6.71q)^4]^{-0.25} \quad (3)$$

where $q = k/(\Omega_m h^2)$. A potential problem with the BBKS transfer function is that it underestimates power on large scales. In the Appendix we investigate the effect that our choice for the CDM transfer function may have on the number of Milky Way satellites. We run one of our simulations adopting the transfer functions from Eisenstein and Hu [32] and we find that this does not affect our results on the number of satellites. We also ran additional CDM simulations (*set C*) using the transfer function calculated by the LINGER program in the GRAFIC2 package ($\Omega_b = 0.04$ was used for calculating the effects of baryons on the matter transfer function). LINGER integrates the linearized equations of general relativity, the Boltzmann equation, and the fluid equations governing the evolution of scalar metric perturbations, photons, neutrinos, baryons, and CDM. The mass and circular velocity functions for satellites are consistent across both transfer functions.

Assuming the WDM to be a thermal particle, a particle that was in thermal equilibrium with the other particle species at the time of its decoupling, we used the transfer function valid for thermal particles given by Bode, Ostriker, and Turok [10]:

$$T_{WDM}(k) = [1 + (\alpha k/h)^\nu]^{-\mu}, \quad (4)$$

where $\nu = 2.4$, $\mu = 4.167$ and

$$\alpha = 0.0516 \left(\frac{m_{WDM}}{1 \text{ keV}} \right)^{-1.15} \left(\frac{\Omega_m}{0.238} \right)^{0.15} \left(\frac{h}{0.73} \right)^{1.3} \left(\frac{g_X}{1.5} \right)^{-0.29}. \quad (5)$$

The parameter g_X is the number of degrees of freedom for the WDM particle, conventionally set to the value for a light neutrino species: $g_X = 1.5$. The parameter k is the spatial wavenumber in Mpc^{-1} and m_{WDM} is the mass of the WDM particle in keV.

A candidate for a thermal WDM particle is the gravitino, the superpartner of the graviton in supersymmetry theories. The lightest stable particle (LSP) in supersymmetry theories is a natural dark matter candidate. If the scale where supersymmetry is spontaneously broken is $\lesssim 10^6$ GeV, as predicted by theories where supersymmetry breaking is mediated by gauge interactions, then the gravitino is likely to be the lightest stable particle and can have a mass reaching into the keV regime [33].

In general the dark matter particle may not have been in thermal equilibrium when it decoupled. This is the case for a sterile neutrino (see [34] and references therein), a theoretical particle added to standard electroweak theory, the only matter it interacts with (except through gravity) is left-handed neutrinos. Sterile neutrinos have been proposed [35–42] as an explanation for the anomalous excess of oscillations observed between muon and electron neutrinos and antineutrinos [43–49]. There are several mechanisms by which sterile neutrinos can be produced. In the standard mechanism proposed by Dodelson and Widrow (DW) [50], sterile neutrinos are produced when oscillations convert some of the more familiar active neutrinos into the sterile variety. The amount produced depends on the sterile neutrino mass and the mixing angle but we will not consider such details here and when considering sterile neutrinos we simply assume they compose the entirety of the dark matter. The transfer function for DW sterile neutrinos with mass m_s is given by [51]

$$T_s(k) = [1 + (\alpha k/h)^\nu]^{-\mu}, \quad (6)$$

where $\nu = 2.25$, $\mu = 3.08$, and

$$\alpha = 0.1959 \left(\frac{m_s}{1 \text{ keV}} \right)^{-0.858} \left(\frac{\Omega_m}{0.238} \right)^{-0.136} \left(\frac{h}{0.73} \right)^{0.692}. \quad (7)$$

Viel et al. [52] give a scaling relationship between the mass of a thermal particle and the mass of the DW sterile neutrino for which the transfer functions are nearly

identical:

$$m_s = 4.379 \text{ keV} \left(\frac{m_{WDM}}{1 \text{ keV}} \right)^{4/3} \left(\frac{\Omega_m}{0.238} \right)^{-1/3} \left(\frac{h}{0.73} \right)^{-2/3} \quad (8)$$

Other sterile neutrino production mechanisms include that of Shi and Fuller (SF) [53] who showed the DW mechanism is altered in the presence of a universal lepton asymmetry where production can be enhanced by resonance effects. Sterile neutrinos can also be produced from decays of gauge-singlet Higgs bosons at the electroweak scale [54]. The momentum distribution of the sterile neutrinos depends on the production mechanism. In the absence of transfer function calculations we use the expressions in [34] for the free streaming length and average momentum to derive approximate scaling factors for the SF and Higgs produced sterile neutrinos: $m_{DW}/m_{SF} = 1.5$, $m_{DW}/m_{Higgs} = 4.5$.

There are also ways other than WDM to reduce small scale power. Broken-scale invariance inflation models [55] have a cutoff length below which power is suppressed. Particle theories where the LSP dark matter particle arises from the decay of the next lightest supersymmetric particle (NLSP) can also suppress small scale power if the NLSP is charged and coupled to the photon-baryon plasma [56] or if the NLSP decay imparts a large velocity to the LSP [57]. Further possibilities include composite dark matter models where stable charged heavy leptons and quarks bind to helium nuclei by Coulomb attraction and can play the role of dark matter with suppression of small scale density fluctuations [58–64]. Our method can potentially be applied to constrain these models as well. However, in the rest of this paper we will not discuss further the consequences that our work has on these theories.

In our simulations we assume the dark matter is thermal and scale the results to the standard sterile neutrino mass using Eq. (8). Our initial conditions include particle velocities due to the gravitational potential using the Zeldovich approximation but we do *not* add random thermal velocities appropriate for WDM to the simulation particles. Bode, Ostriker, and Turok [10] argue that for warm particle masses greater than 1 keV thermal motions are unimportant for halos on scales of a kiloparsec and above. Regardless, we expect thermal motions, if anything, would reduce the number of small mass halos and by not including thermal motions the mass limits derived from our simulations will be more conservative.

We ran simulations for CDM and WDM cosmologies with particle masses of $m_{WDM} = 1, 2, 3, 4,$ and 5 keV ($m_s = 4.4, 11.0, 18.9, 27.8, 37.4$ keV). Figure 2 shows the power spectra for these cosmologies along with the spectrum for an 11 keV standard sterile neutrino using Eq. (8). We ran two separate sets of simulations both consisting of a comoving cubic box 90 Mpc on a side. *Set A* consisted of 204^3 particles giving a ‘coarse’ particle mass of $3.0 \times 10^9 M_\odot$ and a force resolution of 8.8 kpc (all our force resolutions were fixed in comov-

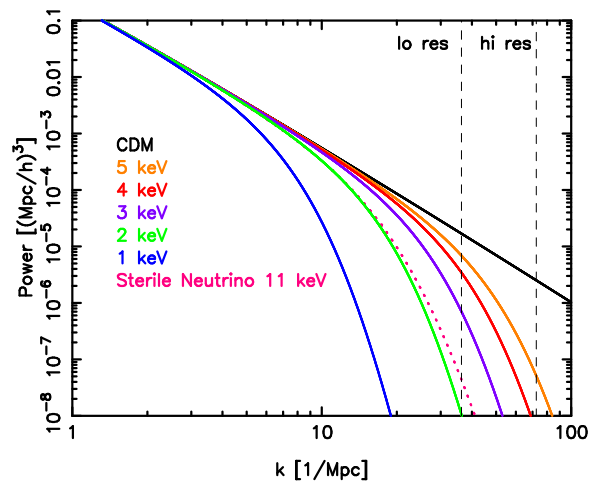


FIG. 2. Power spectra for our simulations. The dotted line is the power spectrum for an 11 keV standard sterile neutrino from Abazajian [51]. The neutrino spectrum is approximately the same as a 2 keV thermal particle, validating the scaling relation of Viel et al. [52]. The vertical dashed lines indicate the lattice cell size in our high and low resolution refinement levels.

ing coordinates). We ran the HOP halo finding software [65] at $z = 0$ and identified Milky Way-sized halos with masses $1 - 2 \times 10^{12} M_\odot$. Halos were examined visually, one was chosen that was at least several Mpc away from clusters and other large structures so as to be relatively isolated. Its particles were identified in the initial conditions and a cubic refinement level, 6.2 Mpc on a side, was placed on the region. For the refinement region in our low resolution simulations we used 11, 239, 424 (224^3) particles with mass and force resolutions of $7.3 \times 10^5 M_\odot$ and 550 pc, respectively. For CDM and WDM particle masses of 1, 2, and 4 keV we also conducted higher resolution simulations with 89, 915, 392 (448^3) particles in the refinement region and mass and force resolutions of $9.2 \times 10^4 M_\odot$ and 275 pc, respectively. The simulated Milky Way halo had a neighbor halo with mass $0.23 M_{MW}$ at a distance of 700 kpc in the low resolution simulations. The real Milky Way has a massive neighbor in M31, the Andromeda galaxy ($M_{M31} \sim 1 - 3 M_{MW}$), at a distance ~ 700 kpc. Being nonlinear and chaotic systems, small perturbations to the trajectories of dark matter halos can be amplified exponentially and in the higher resolution simulation this satellite is merging with the Milky Way at $z = 0$. Such a merger may disrupt the equilibrium of the halo and make it nonrepresentative of the actual Milky Way. The difference between the high and the low resolution simulations is significant and complicates the comparison between the resolutions; however, this merger is not a violation of the selection method used for the *set C* halos described below and we find excellent agreement across all simulation sets.

The need to explore the scatter between the subhalo distributions of different realizations of Milky Way-type halos, in addition to the complications arising with the

high and low resolution simulations of *set A*, prompted us to conduct a second set of simulations. *Set B* consisted of 408^3 particles giving a coarse particle mass of $3.8 \times 10^8 M_\odot$ and a force resolution of 4.4 kpc. We ran HOP and identified halos with masses $0.8 - 2.2 \times 10^{12} M_\odot$. For each halo we also found the nearest neighboring halo with mass $> 0.8 \times 10^{12} M_\odot$. We selected a halo whose nearest massive neighbor was at least 5 Mpc away and visually verified the halo was indeed isolated. A rectangular refinement level $6.1 \times 7.0 \times 7.9$ Mpc was placed over this halo's particles in the initial conditions. Low and high resolutions were conducted with the same mass and force resolutions as *set A*. The low resolution simulations used 16,515,072 ($\sim 255^3$) particles in the refinement level while high resolution used 132,120,576 ($\sim 510^3$) particles in the refinement level.

A third set of CDM only, low resolution simulations was run to further explore the scatter between the subhalo distributions of different realizations of Milky Way-type halos and to explore the possibility of a bias introduced by the use of the BBKS transfer function. *Set C* consisted of 408^3 particles but the CDM transfer function was generated from the LINGER software in GRAFIC2 [30] after correcting a bug where the power spectrum for baryons was used for dark matter when calculating the transfer function. We used the AMIGA's Halo Finder (AHF) software [66] to find MW-sized halos with no equal sized neighbor within two virial radii (defined below). Nine halos were selected for refinement at low resolution from a variety of environments, low density with few large halos to high density with many large halos. The rectangular refinement regions had lengths 7.5 – 15.8 Mpc and 31,752,192 – 69,009,408 ($316^3 - 410^3$) particles.

Table I summarizes the properties calculated by AHF for all of our simulated Milky Way halos at $z = 0$. We write R_Δ to mean the radius enclosing an overdensity Δ times the critical value. The mass and number of particles inside R_Δ are M_Δ and N_Δ , respectively; v_Δ is the circular velocity $v_\Delta^2 \equiv GM_\Delta/R_\Delta$ at R_Δ , and v_{max} is the maximum circular velocity of the halo. We use the value $\Delta = 178\Omega_m^{0.4} = 100$ [67] (which is also very close to the value using the definition from [68]) for the virial radius of our MWs and consider subhalos within R_{100} when comparing to other published work. The mass, radius, and velocity at $\Delta = 50$ are also used in the literature and these values are also listed in Table I.

Figure 3 shows the density profiles of the *A* and *B* Milky Way halos calculated by breaking the halos into spherical shells. Small differences between the high and low resolution *set A* halos caused by the merging neighbor are apparent but generally the profiles are very similar across all simulations of each set. We do not see an inner flattening of the halos in the WDM simulations because we did not add thermal motions to our particles. Figure 4 shows portraits of the Milky Way in our *set B* high resolution simulations.

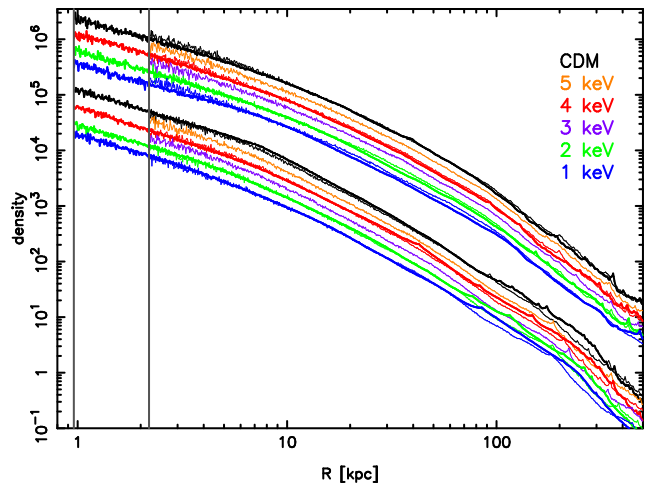


FIG. 3. Density profile of Milky Way halos in the *set A* and *set B* CDM and WDM simulations. Thick lines are the high resolution simulations. *Set B* simulations are at top, the *set A* and the WDM cosmologies in each set have been offset downward for clarity. The profiles are plotted starting from the convergence radius of Power et al. [69] for both resolutions (vertical lines).

A. Identification of Satellites

We used the AHF halo finding software [66] to find the gravitationally bound dark matter halos in our N -body simulations. Unbound particles were iteratively removed and we selected gravitationally bound halos with ten or more particles.

AHF calculates properties of the halos it finds such as the total mass and the maximum circular velocity. For our purposes the maximum circular velocity is a better characteristic of a subhalo than the mass because quantifying the outer boundary of a subhalo embedded in a larger halo is somewhat arbitrary and can introduce systematic errors. The maximum circular velocity however typically occurs at a radius well inside the subhalo outskirts.

III. RESULTS

A. Satellite Distribution Functions

We first compare our CDM simulations to other CDM simulations in the literature. Figure 5 shows the cumulative mass functions, $N(> M_{sub})$, for subhalos within R_{50} for the *set A* and *B* MWs. Poisson statistic error bars have been added to the high resolution simulations and fit by $N \propto M^{-\beta}$. The values of β (0.9 and 0.95) agree with other published work that find values of 0.7 – 1.0 [2, 70–77]. At both high and low resolution the simulated mass functions turn away from the fit at masses below about 200 times the mass resolution of the simulation; this was also seen in the Via Lactea simulation [75]. Also

TABLE I. Properties of simulated Milky Way halos.

Simulation	M_{100} [$10^{12} M_{\odot}$]	R_{100} [kpc]	M_{50} [$10^{12} M_{\odot}$]	R_{50} [kpc]	v_{50} [km/s]	v_{max} [km/s]	N_{100}	N_{50}
<i>Set A</i>								
CDM lo	1.4867	288.25	1.6786	378.47	138.11	183.02	2,026,414	2,287,923
5 keV lo	1.4964	288.86	1.6825	378.75	138.22	183.38	2,039,597	2,293,239
4 keV lo	1.5060	289.45	1.6833	378.82	138.24	183.87	2,052,643	2,294,398
3 keV lo	1.5141	290.00	1.6850	378.95	138.29	182.98	2,063,747	2,296,714
2 keV lo	1.5100	289.74	1.6702	377.84	137.88	181.59	2,058,104	2,276,518
1 keV lo	1.4983	289.00	1.6615	377.18	137.64	180.04	2,042,264	2,264,672
CDM hi	1.8403	309.49	2.0331	403.43	147.22	191.94	20,067,182	22,169,072
4 keV hi	1.8261	308.70	2.0383	403.77	147.34	189.69	19,911,999	22,225,367
2 keV hi	1.8326	309.06	2.0266	402.99	147.06	183.82	19,982,705	22,098,268
1 keV hi	1.8373	309.33	2.0244	402.85	147.01	179.39	20,033,935	22,073,940
<i>Set B</i>								
CDM lo	1.9005	312.84	2.1325	409.89	149.58	195.87	2,590,475	2,906,549
5 keV lo	1.8862	312.04	2.1254	409.44	149.41	195.76	2,570,982	2,896,920
4 keV lo	1.8863	312.04	2.1212	409.16	149.32	195.84	2,570,992	2,891,165
3 keV lo	1.8800	311.70	2.1185	409.00	149.25	195.75	2,562,445	2,887,566
2 keV lo	1.8479	309.92	2.0936	407.38	148.67	195.24	2,518,690	2,853,610
1 keV lo	1.8263	308.70	2.0752	406.19	148.23	192.33	2,489,258	2,828,485
CDM hi	1.7533	304.53	1.9948	400.88	146.29	194.01	19,117,720	21,751,717
4 keV hi	1.7426	303.92	1.9781	399.75	145.88	188.52	19,001,776	21,569,680
2 keV hi	1.7288	303.11	1.9640	398.81	145.53	185.18	18,850,480	21,415,983
1 keV hi	1.6230	296.80	1.8655	392.01	143.06	179.59	17,697,389	20,341,369
<i>Set C</i>								
CDM lo 1	2.4814	342.19	2.8071	449.22	163.93	214.42	3,351,495	3,761,164
CDM lo 2	2.3512	336.10	2.8287	450.37	164.35	213.86	3,204,746	3,855,526
CDM lo 3	1.9846	317.63	2.2133	415.01	151.45	203.23	2,705,093	3,016,787
CDM lo 4	2.2587	331.63	2.6486	440.60	160.79	199.95	3,078,658	3,610,116
CDM lo 5	1.7665	305.53	1.9226	345.21	154.77	193.06	2,382,645	2,589,405
CDM lo 6	1.6004	295.64	1.8977	394.26	143.88	187.76	2,174,733	2,567,693
CDM lo 7	1.8704	311.41	2.7754	447.52	163.31	187.56	2,549,352	3,782,898
CDM lo 8	1.9858	317.70	2.3401	422.78	154.29	194.43	2,706,610	3,189,609
CDM lo 9	1.6881	300.95	1.8936	393.97	143.77	201.23	2,300,887	2,581,006

plotted are the mass functions for the *set C* simulations. The subhalo abundances of the *set A* and *B* halos are within the halo to halo scatter and are consistent with the *set C* simulations.

The cumulative maximum circular velocity functions for subhalos within R_{100} are plotted in Figure 6. The maximum velocities of the subhalos have been normalized by the maximum circular velocity of their host MW. The shaded region shows the minimum and maximum (lighter) and $\pm 1\sigma$ (darker) from the mean of the 68 halos with masses $1.5 - 3 \times 10^{12} M_{\odot}$ in the simulation of Ishiyama et al. [78]. We use the fit to the density profile of the Via Lactea II halo [29] to estimate its R_{100} (298 kpc) and from the published subhalo catalog we cal-

culate and plot the Via Lactea II velocity function as the dashed line. The solid straight line is the fitting formula from the Bolshoi simulation [79],

$$N(> x) = 1.7 \times 10^{-3} v_{max,host}^{1/2} x^{-3}, \quad (9)$$

$$x \equiv v_{max}/v_{max,host}, \quad (10)$$

applied to our high resolution halos which provides an excellent fit (the difference between the fit for the *set A* and *B* $v_{max,host}$ is less than the thickness of the line). Via Lactea II used the same cosmological parameters as our simulations and their subhalo abundance agrees well with our simulations. Our simulations are consistent with the Ishiyama et al. simulation but are systematically on

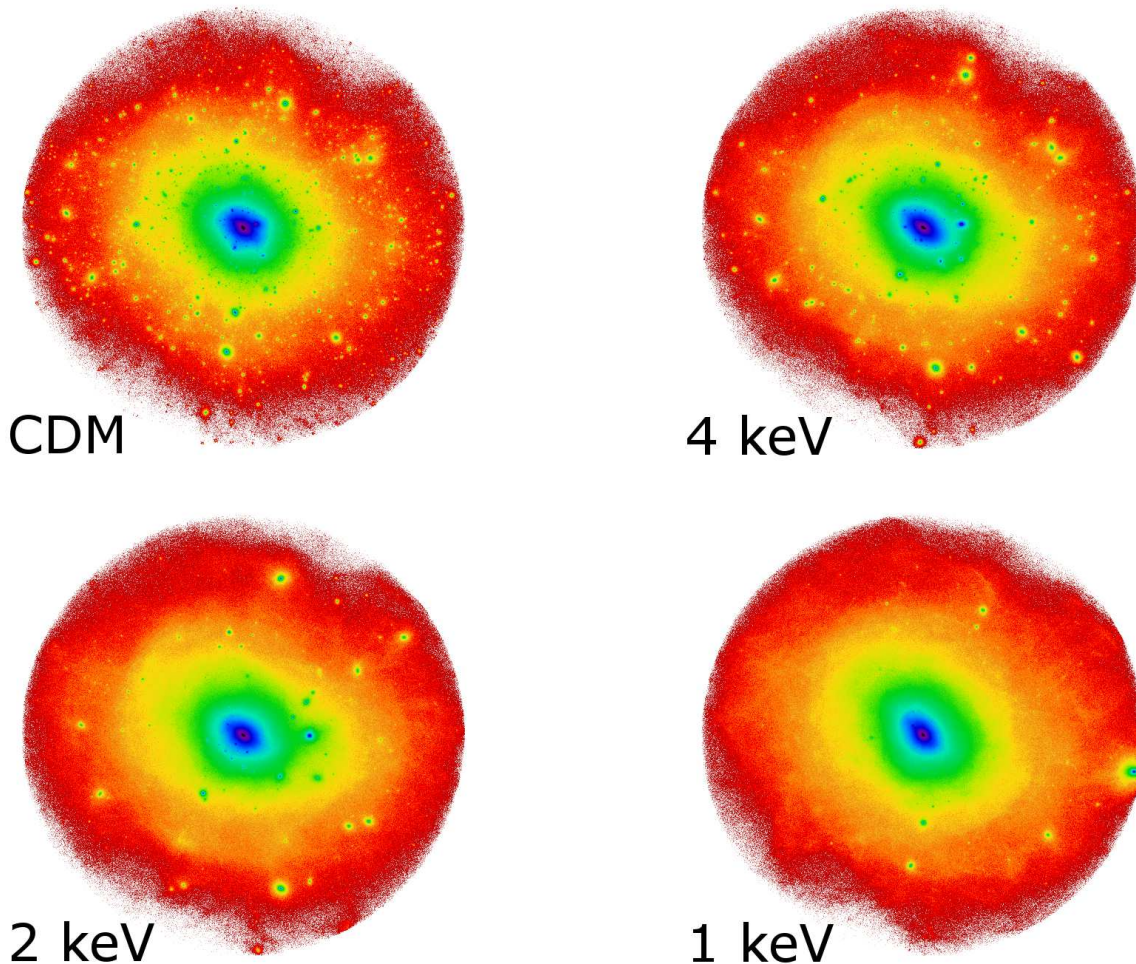


FIG. 4. Portraits of the simulated Milky Way halo at $z = 0$ in the *set B* high resolution simulations. Structure within 500 kpc of the MW centers is shown.

the low end of their distribution. This is likely due to the different cosmology used in the Ishiyama et al. simulation (discussed below).

Figure 7 also plots the cumulative velocity functions but includes all subhalos within R_{50} and the subhalo velocities have been normalized by the circular velocity at R_{50} of their host MW. The Ishiyama et al. halos are again plotted as in Figure 6 as well as Via Lactea II. The solid straight line is the result from the Aquarius simulations [77]. Again there is good agreement between our simulations and Via Lactea II but an offset between our simulations and those of Ishiyama et al. and Aquarius. To first order, the abundance of halos of any size depends on the power spectrum of density perturbations which depends on the normalization, σ_8 , and the tilt of the power spectrum, n_s . Larger values of either parameter increases the power on small scales and leads to a larger number of satellites for a given mass and v_{max} of the host. The values ($\sigma_8 = 0.9$, $n_s = 1$) were used in the Aquarius simulations and (0.8, 1) were used by Ishiyama

et al. Both are significantly greater than our adopted values of (0.74, 0.951), and this is the likely cause of the abundance offset.

We adopted a WMAP3 cosmology to facilitate comparison to the Via Lactea II simulation. The WMAP3 values of n_s , σ_8 , and Ω_m are 1.0, 2.9, and 2.5 standard deviations below the latest WMAP7 values [80]. The Bolshoi simulation used parameters in agreement with WMAP7 and constraints from other cosmology projects. A comparison of the subhalo abundances of 4960 Bolshoi halos with circular velocities and masses comparable to the Via Lactea II halo indicated Bolshoi has more subhalos by about 10%. Although Via Lactea II is just one halo and may not be representative of the average for a WMAP3 cosmology, this agrees with expectations from the 10% smaller value of σ_8 used by Via Lactea II. We used the same value of σ_8 as Via Lactea II but the Bolshoi fitting formula applied to our high resolution simulations in Figure 6 provides an excellent fit with no indication of an offset. This could be because, as we show in the

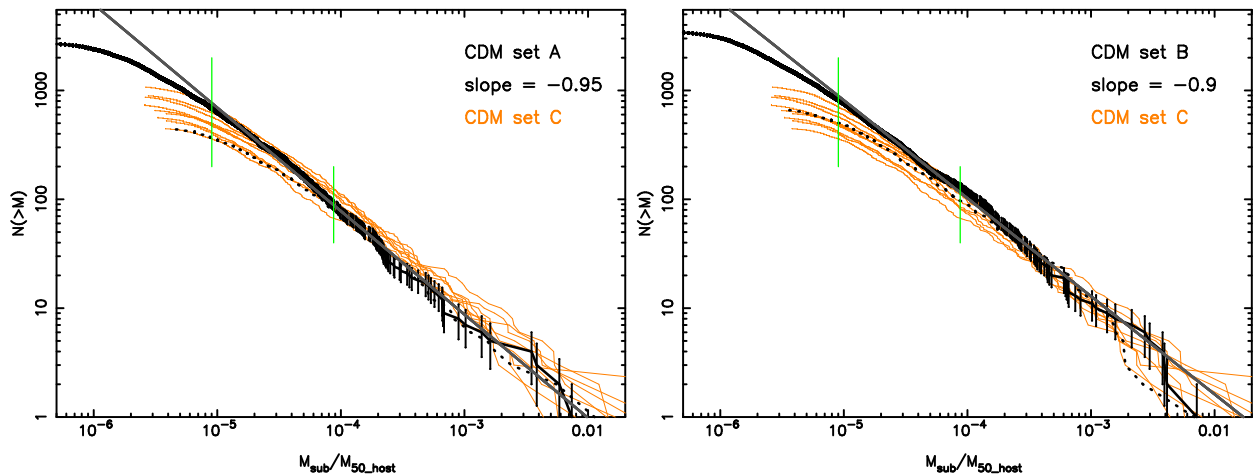


FIG. 5. Cumulative mass functions for subhalos within R_{50} for the CDM *set A* (left) and *set B* (right) simulations. Subhalo masses have been normalized by the M_{50} mass of the host. Poisson error bars have been added to the high resolution simulations and fit with a straight line. Both high and low resolution (dotted lines) turn away from the straight fit below about 200 times the mass resolutions of the simulations (short vertical lines). Mass functions for the *set C* halos have also been added (thin lines) and show the *A* and *B* abundances are within the halo to halo scatter.

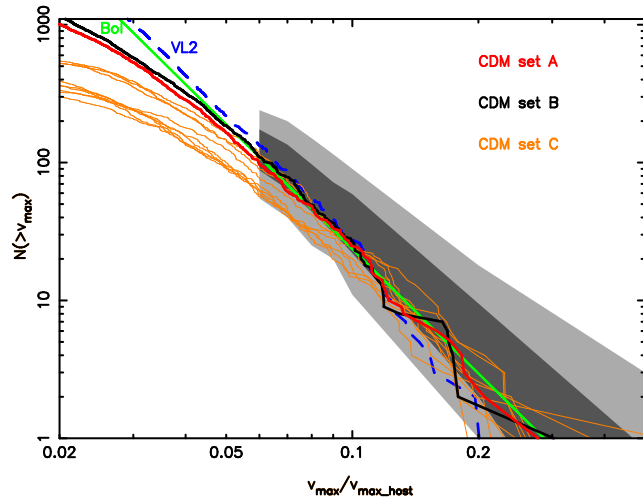


FIG. 6. Cumulative velocity functions for subhalos within R_{100} in our low resolution *set C* (thin lines) and high resolution *set A* and *set B* (thick lines) MW halos. Subhalo circular velocities have been normalized to the maximum circular velocity of the host halo. The dashed line is the subhalo velocity function of Via Lactea II, the straight solid line is the fitting formula from the Bolshoi simulation applied to our *A* and *B* halos. The shaded regions show the minimum and maximum and $\pm 1\sigma$ from the mean of the 68 MW-sized halos of Ishiyama et al. [78]

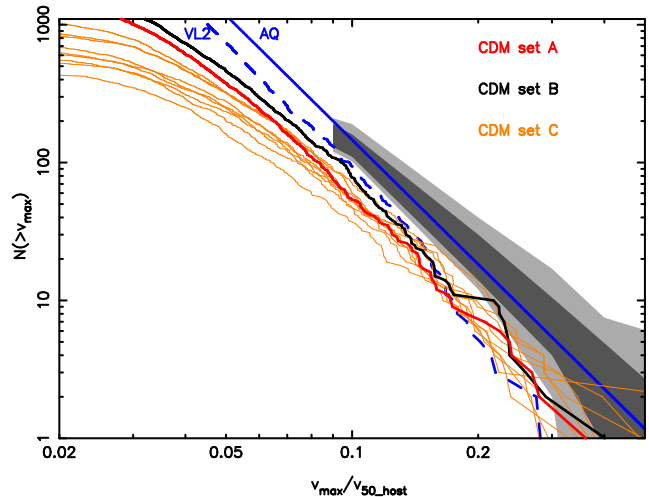


FIG. 7. Cumulative velocity functions for subhalos within R_{50} in our low resolution *set C* (thin lines) and high resolution *set A* and *set B* (thick lines) simulations. Subhalo circular velocities have been normalized to the circular velocity of the host halo at a radius enclosing an overdensity of $\Delta = 50$. The dashed line is the velocity function for Via Lactea II and the straight solid line is the average abundance from the Aquarius simulations [77]. The shaded region is the minimum/maximum range and $\pm 1\sigma$ about the mean for halos from the simulations of Ishiyama et al. [78].

Appendix, the BBKS power spectrum used in our high resolution simulations has about 10% more power at sub-Galactic scales. Below we argue that an intrinsic scatter in subhalo abundance of 30% (1σ) is reasonable to adopt and we conclude this can account for variations in the adopted cosmology without the need for a separate correction.

From our simulations and those of Ishiyama et al. in Figures 6 and 7 it is clear that the subhalo abundances of halos of similar sizes have a scatter. For a given cosmology the scatter in abundance includes an intrinsic scatter and a statistical scatter from the number of subhalos. The Aquarius simulation suite included 6 MW-sized halos simulated at very high resolution. For subhalos within

R_{50} , at high values of the abundances where the statistical scatter is small, the 1σ intrinsic scatter was determined to be 10%. In Figure 7 the scatter in the Ishiyama et al. abundances decreases for increasing N and appears to be converging to the 10% found in Aquarius. However the variation in the Ishiyama et al. abundances in Figure 6 is clearly converging to a larger value. As argued in [78], the smaller scatter in Figure 7 can be explained by the inclusion of subhalos at distances up to R_{50} which are outside the virial radius and, hence, their evolution has not been affected by the structure of the host halo. Using v_{50} to normalize the subhalo velocities can also reduce scatter since, unlike v_{max} , it is less dependent on the central concentration. We will be interested in the number of subhalos in the inner regions of the host MW which are expected to be sensitive to the host concentration so we will adopt the higher value for the intrinsic variation in the number of subhalo from Figure 6 which we estimate to be about 30% (1σ) after subtracting the Poissonian statistical scatter expected from the number of subhalos.

In Figure 8 the cumulative circular velocity functions for subhalos within R_{100} for the high resolution *set A* and *set B* CDM and WDM simulations are plotted. The *set A* abundances have been increased 7% to normalize the CDM abundances to those of the *set B* simulation and illustrate that the relative suppression of subhalo abundances for each WDM simulation compared to CDM is the same across both simulation sets. The straight line is the Bolshoi fitting function applied to the *set B* CDM halo. The vertical lines in Figure 8 show where $v_{max} = 6$ and 8 km/s. Below 8 km/s the high resolution CDM simulations begin to fall away from the Bolshoi line due to the resolution limits of the simulations. For $v_{max} > 8$ km/s our simulations are reasonably complete within R_{100} of each Milky Way although numerical destruction of a small fraction of satellites in the inner Milky Way would not be apparent in Figure 8, especially for the CDM and 4 keV cosmologies. Before comparing our simulations to observations we need to determine to what distance our simulations are convergent.

B. Convergence Study

Satellites orbiting in the halo of a larger galaxy are destroyed by tidal stripping and heating through encounters with other satellites. Satellites in simulations are also destroyed artificially by numerical effects that become dominant for poorly resolved halos in the inner halo region. There will therefore be a radius inside of which our simulations will not converge to a realistic representation of the actual Milky Way.

To determine the convergence of our simulations and have an idea of the variance of the results, we performed simulations at lower and higher resolution of two different realizations of a Milky Way-sized galaxy. We performed convergence studies following the argument elu-

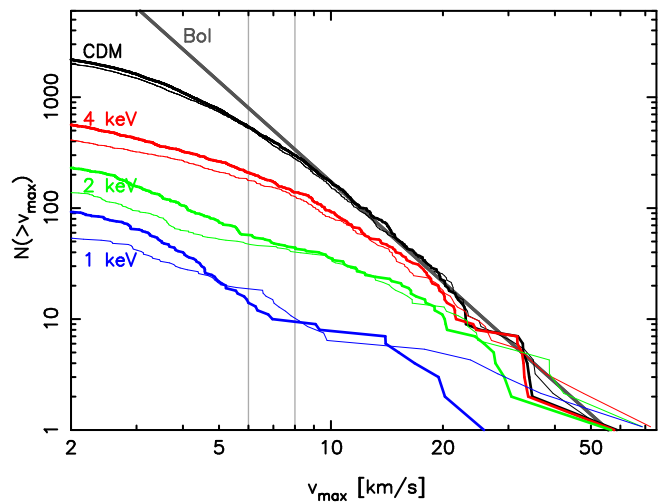


FIG. 8. Cumulative velocity functions for satellites in our high resolution *set A* and *set B* CDM and WDM simulations. The *set A* abundances (thin lines) have been increased by 7% to normalize the CDM abundances to those of the *set B* and show that the relative suppression of halos in WDM cosmologies compared to CDM is similar across both simulations. The straight gray line is the Bolshoi fitting formula applied to the *set B* halo.

cidated below, in combination with results of published high resolution simulations found in the literature. Using the work of Moore et al., De Lucia et al., and Ishiyama et al. [2, 73, 78], we will assume that the shape of the cumulative satellite velocity function for host halos of different masses is nearly constant and the total number of satellites scales linearly with the host mass. If the simulations are convergent, the cumulative circular velocity function for satellites, $N(R)$, within a given Galactocentric radius, R , should be proportional to the enclosed mass, $M(R)$, and a function of R that represents the fraction of satellites that survive destruction from physical effects:

$$N(R) \equiv f(R)M(R), \quad (11)$$

where $f(R) \propto R^\alpha$. The normalization of $f(R)$ can be set using values of $N(R)$ and $M(R)$ at a distance R_0 :

$$N(R) \left(\frac{R_0}{R} \right)^\alpha \left(\frac{M_0}{M(R)} \right) = N_0 = const. \quad (12)$$

The velocity functions normalized in this way will be constant with radius where the simulations are convergent. Where numerical effects destroy satellites the velocity functions will normalize to a lower value. We expect that α is constant because there is no characteristic scale for the destruction rate in dark matter only simulations. Hence, α can be determined at large radii where convergence is certain.

Figure 9 shows the normalized velocity functions for the simulations. The normalization constants M_0, R_0 have been chosen at 200 kpc and the value of α (0.55) was adjusted by hand until a good fit was achieved for

the *set B* velocity functions above 200 kpc in the high resolution CDM cosmology at circular velocities > 6 km/s (vertical lines). This α also provides a good fit for the WDM cosmologies and for the *set A* simulations, although the 1 and 2 keV velocity functions have a wider scatter due to the smaller numbers of satellites in these simulations. The $m_{WDM} = 4$ keV simulation is convergent for $v_{max} > 6$ km/s to distances > 100 kpc. At 75 kpc the effects of numerical resolution are apparent. The same value of α has been used in the normalization of the low resolution sets and appears to provide a good fit for the velocity functions $> 200 - 250$ kpc. The effects of numerical resolution on the destruction of satellites are apparent at larger distances in these simulations: < 200 kpc for CDM and < 150 kpc for WDM.

The 1 and 2 keV WDM velocity functions in Figures 8 and 9 show a flattening when going from high to low velocities until about 6 km/s, below which the number of subhalos increases greatly. This is a generic feature of WDM simulations [10, 81] and is usually explained as top-down fragmentation of matter filaments. Given that WDM simulations are known to form nonphysical halos along filaments [24, 25], it is likely the low velocity upturn in the velocity function of subhalos is actually caused by these numerical artifacts accreting onto the MW. Since these nonphysical halos form with separations typical of the mean particle distances in the initial conditions, the number of halos should increase with the mass resolution of the simulation. Our low resolution simulations do not show clear evidence of upturns in the velocity functions, we require simulations with resolution higher than our high resolution sets to confirm this effect. Regardless, we consider only satellites with velocities greater than 6 km/s in our high resolution simulations when deriving our constraints on the dark matter particle mass.

C. Comparison to Observations

Before the Sloan Digital Sky Survey there were only 12 classically known satellite galaxies to the Milky Way. Sixteen new satellites have been discovered in the SDSS, currently in Data Release 7. We list all known Milky Way satellites in Table II. We use the satellite distances given in Table II as their Galactocentric distances. When comparing the observed satellites to the simulations, we must correct the SDSS dwarfs for completeness. The primary incompleteness of the SDSS is its sky coverage, 28.3% (11663 deg²). Second, being a magnitude limited survey, the SDSS has a luminosity bias. The detection efficiency of dwarfs in the SDSS is a function of dwarf size, luminosity, distance, and Galactic latitude as shown by Walsh et al. [82]. An approximate expression is given in Tollerud et al. [83] (using the work of Koposov et al. [84]) for the distance which galaxies of luminosity $> L$ are completely detected: $d \approx 66\text{kpc}(L/1000 L_{\odot})^{1/2}$. Galaxies with $L > 10^4 L_{\odot}$ should be approximately complete to 200 kpc, with $L > 2300 L_{\odot}$ to 100 kpc. The distance

range 100–200 kpc is thus suited for comparisons because our simulations are convergent and the observations are nearly, but not quite, complete. For our analysis we will only use satellites with distances < 200 kpc. For compar-

TABLE II. Summary of known Milky Way satellites.

Name	$dist$ [kpc]	σ_{star} [km/s]	M_V	References
Classical (pre-SDSS)				
Sagittar	24 ± 2	11.4 ± 0.7	-13.4	[85]
LMC	49 ± 2	...	-18.4	[85]
SMC	58 ± 2	...	-17.0	[85]
Ursa Minor	66 ± 3	9.3 ± 1.8	-8.9	[85]
Draco	79 ± 4	9.5 ± 1.6	-8.8	[85]
Sculptor	79 ± 4	6.6 ± 0.7	-11.1	[85]
Sextans	86 ± 4	6.6 ± 0.7	-9.5	[85]
Carina	94 ± 5	6.8 ± 1.6	-9.3	[85]
Fornax	138 ± 8	10.5 ± 1.5	-13.2	[85]
Leo II	205 ± 12	6.7 ± 1.1	-9.6	[85]
Leo I	270 ± 30	8.8 ± 0.9	-11.9	[85]
Phoenix	405 ± 15	...	-10.1	[85]
SDSS discovered				
Segue I	23 ± 2	4.3 ± 1.2	-1.5	[86]
Ursa Major II	30 ± 5	6.7 ± 1.4	-3.8	[87, 88]
Segue II	~ 35	3.4 ± 2.0	-2.5	[89]
Willman I	38 ± 7	$4.3^{+2.3}_{-1.3}$	-2.5	[87, 90]
Coma Berenics	44 ± 4	4.6 ± 0.8	-3.7	[88, 91]
Bootes II	60 ± 10	...	-3.1	[92]
Bootes I	62 ± 3	$6.5^{+2.0}_{-1.4}$	-5.8	[87]
Pisces I	80 ± 14	[93, 94]
Ursa Major I	106^{+9}_{-8}	7.6 ± 1.0	-5.6	[88]
Hercules	140^{+13}_{-12}	5.1 ± 0.9	-6.0	[88, 91]
Canes Venatici II	150^{+15}_{-14}	4.6 ± 1.0	-4.8	[88, 91]
Leo IV	160^{+15}_{-14}	3.3 ± 1.7	-5.8	[88, 91]
Leo V	175 ± 9	2.4 ± 1.8	-5.2	[95, 96]
Pisces II	~ 180	...	-5.0	[97]
Canes Venatici I	220^{+25}_{-16}	7.6 ± 0.4	-7.9	[88, 98]
Leo T	~ 420	7.5 ± 1.6	-7.1	[88, 99]

ison with the simulations, we do a first order correction for the sky coverage of the SDSS assuming an isotropic distribution of satellites. The SDSS covers 0.283 of the sky, so for every satellite detected we assume there are actually 3.54 satellites at that distance. Combined with the classic Milky Way satellites this forms our observed data set. We also implemented a conservative luminosity correction for the SDSS dwarfs using the formulas in Walsh et al. [82]. This adds two satellites making a total of 61 ± 13 satellites within 200 kpc where the error only includes Poisson statistics of the SDSS dwarfs: $3.54\sqrt{N_{SDSS}}$. The extra two satellites are at distances 150–200 kpc and do not affect our conclusions. We note

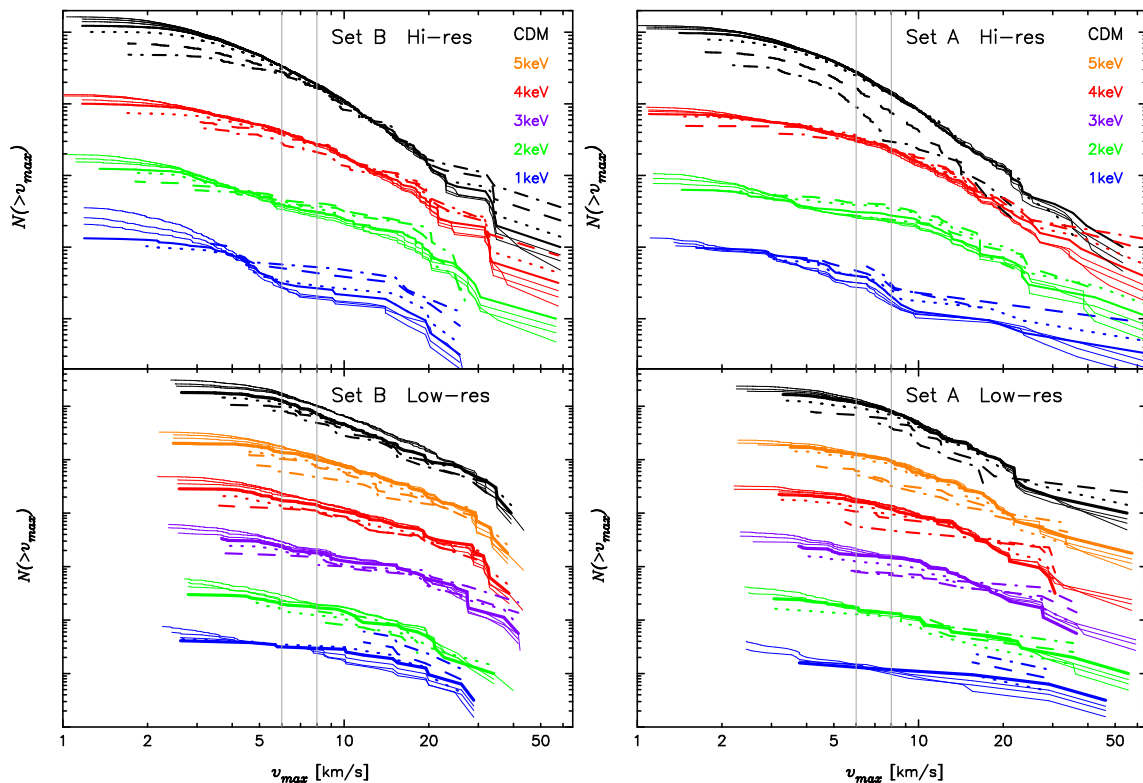


FIG. 9. (left) Velocity functions for *set B* high (top) and low (bottom) resolution simulations normalized with Eq. (12). Solid lines are $R = 400, 300, 250,$ and 200 kpc (thick), dotted line is $R = 150$ kpc, dashed line is $R = 100$ kpc, dot-dashed line is $R = 75$ kpc. The WDM cosmologies have been shifted down vertically for clarity. The value $\alpha = 0.55$ was set by the high resolution simulation and provides good normalization for the low resolution as well but the effects of incompleteness become apparent at much larger radii ($150 - 200$ kpc compared to $75 - 100$ kpc for high resolution). (right) Same as the left panel, but for the *set A* high (top) and low (bottom) resolution simulations. The value $\alpha = 0.55$ also provides good normalization for this set of halos.

that we get the same result if we only include dwarfs detected in the Data Release 5 footprint and correct for the smaller sky coverage (8000 deg^2). We also note the formulas in Walsh et al. [82] assume the size-luminosity distribution of known dwarfs is representative of all satellites. There may be a population of dwarfs with surface brightnesses below the detection limit of the SDSS [100–103].

Willman 1 is an exceptional case in that it may not be a dark matter dominated dwarf galaxy but a globular cluster undergoing tidal disruption. Its stellar velocity dispersion implies a large mass to light ratio like other dwarf spheroidals and it has a size and luminosity intermediate between MW dwarfs and globular clusters [90], but unresolved binaries and tidal heating may contaminate the velocity dispersion and lead to an overestimated mass. Although it has a large metallicity spread unlike the stellar population of a globular cluster [87], follow-up spectroscopy [104] suggests there may be contamination by foreground stars and when these are excluded the metallicity spread can be consistent with a metal-poor globular cluster. The detection of an X-ray emission line from decaying dark matter in Willman 1 has been claimed [105, 106] but is provisional [107]. If confirmed

this would indicate a dark matter halo in Willman 1 and confirm its status as a MW satellite. When deriving constraints on the dark matter particle mass we will consider both including and excluding Willman 1 as a Milky Way satellite.

When comparing observations and simulations we will apply cuts to the simulated subhalos and consider only those with velocities above 6 and 8 km/s. As discussed in the previous section this is to avoid potential contamination from numerical effects in the WDM simulations. That these velocity cuts are a reasonable estimate of the minimum v_{max} of the dark matter halos the observed galaxies are presumably embedded in can be shown as follows. Ricotti and Gnedin [100] found in simulations that the maximum circular velocities of satellites are at least twice the velocity dispersion of the stellar component. Assuming the stellar velocity dispersions of the observed dwarfs are $\sqrt{3}$ times the line-of-sight velocity dispersions (σ_{star} in Table II), then all dwarfs with measured velocity dispersions have maximum circular velocities greater than 8 km/s. We assume dwarfs without measured velocity dispersions are similar to the other known dwarfs and conservatively conclude all dwarfs reside in dark matter halos with v_{max} greater than 8 km/s. An alternative ap-

proach is the work of Wolf et al. [108] relating the circular velocity at half light radius to σ_{star} : $v_c(r_{1/2}) = \sqrt{3}\sigma_{star}$. All the observed dwarfs except Leo V have circular velocities at half light radius about 6 km/s or greater. Since the maximum circular velocity must be greater than or equal to the half light circular velocity, it is also reasonable to consider that all observed dwarfs reside in halos with $v_{max} > 6$ km/s. We stress that these cuts reflect the need to reduce the numerical effects of the nonphysical halos in WDM simulations that dominate our high resolution simulations at subhalo velocities below 6 km/s rather than an assumption on the relationship between luminous satellites and dark matter halos.

In the left panel of Figure 10 we plot histograms of the number of satellites with distance for the observed and simulation data sets with a 6 km/s maximum circular velocity cut. The upward arrows on the observed data bars indicate these are only lower limits due to the surface brightness limits of the SDSS; it is possible there are more dwarfs yet to be discovered. Willman 1 has not been included as a MW satellite in this figure. The 6 km/s cut to the simulation data assures the high resolution simulations are convergent to at least $r = 100$ kpc. The low resolution simulations are also plotted in these figures but they are convergent only to 150 kpc. Focusing on the 100 – 200 kpc bins it is clear the 1 keV has far too few satellites to match the observations. The 2 keV simulations are consistent with the observations in the 100 – 150 kpc bin but to be generally consistent with the observations would require the simulations to be significantly incomplete below 100 kpc or the sky correction to have overestimated the number of satellites in the inner Milky Way. The 4 keV simulations can be consistent with the observations although they may require some of the dark matter halos to not host luminous galaxies. Strong conclusions cannot be drawn from this plot because it is not clear how variance in the satellite abundances for the simulated halos may affect the results.

The number of satellites in the simulations can be corrected for completeness using the convergence equation, Eq. (12). We used the mass and number of satellites inside R_{50} for the normalization and calculated the number of satellites in 50 kpc bins for the high resolution simulations. The results are shown in the right panel of Figure 10. The results are very similar across cosmologies, a nearly constant number of satellites per bin from 50 – 200 kpc with about half as many in the 0 – 50 kpc bin. The plots are also very similar to the simulation data plots except for the 0 – 50 kpc bin in the 4 keV cosmology where about ten satellites were destroyed by numerical effects in the *set B* halo. The 0 – 50 kpc bin is most important for constraining the dark matter particle mass because the observations are most complete in this bin.

In the top panel of Figure 11 we plot the number of satellites in the 0 – 50 kpc bin calculated from the convergence equation for the high resolution *set B* Milky Way as a function of the particle mass with a 6 km/s veloc-

ity cut to the subhalos. We set the variance in satellite abundances equal to that for a 30% intrinsic rms scatter plus a Poissonian variance in the number of satellites. The dark and light shaded regions in the plot show the 1σ and 2σ ranges, respectively. The solid horizontal line shows the number of observed satellites after applying sky coverage corrections to the SDSS data (excluding Willman 1) while the dashed and dotted horizontal lines show the 68% and 95% confidence lower limits from Poisson statistics. In the bottom panel of Figure 11 we plot the difference in the number of observed and simulated satellites with 1σ and 2σ limits (shaded regions) from combining the variances of the observed and simulated data sets. The number of satellites in simulation must be at least equal to the number of observed satellites, therefore where this quantity equals zero defines a lower limit on the dark matter particle mass. The arrowed lines indicate the lower limits at 1σ and 2σ for this case of the *set B* simulation with a 6 km/s cut to the subhalos and excluding Willman 1 from the observed set.

We repeated the same analysis using a $v_{max} > 8$ km/s cut to the simulation data. We also considered the effects when Willman 1 was included in the observed data set for both the 6 km/s and 8 km/s analysis. We present the results in Table III. The *set B* halo is slightly more abundant in subhalos but both the *set A* and *B* simulations give the same results to within about 10%. Rather than take the average of the two simulations we will simply adopt the more conservative of the two constraints. In the most conservative case, where Willman 1

TABLE III. Dark matter particle mass constraints (in keV) from the high resolution *set A* and *B* MW halos. Constraints for simulated subhalo v_{max} cuts of 8 and 6 km/s and including or excluding Willman 1 from the observed data set are given.

	$v_{max} > 8$ km/s		$v_{max} > 6$ km/s					
	Included	Excluded	Included		Excluded			
MW	A	B	A	B	A	B		
2σ	> 3.6	> 3.3	> 2.9	> 2.7	> 3.0	> 2.6	> 2.5	> 2.3
1σ	> 5	> 4.6	> 4.2	> 3.8	> 3.9	> 3.4	> 3.3	> 2.9

is not a dark matter dominated dwarf galaxy and all observed satellites correspond to dark matter halos with $v_{max} > 6$ km/s, we can say $m_{WDM} > 2.3$ keV with 95% confidence. We adopt this as our formal limit for this work.

IV. DISCUSSION

We found that a model with $m_{wdm} = 4$ keV produces the best fit to observations at < 50 kpc, i.e. this model has a number of dark matter satellites equal to the number of observed luminous satellites. However, due to the large uncertainties in the number of observed satel-

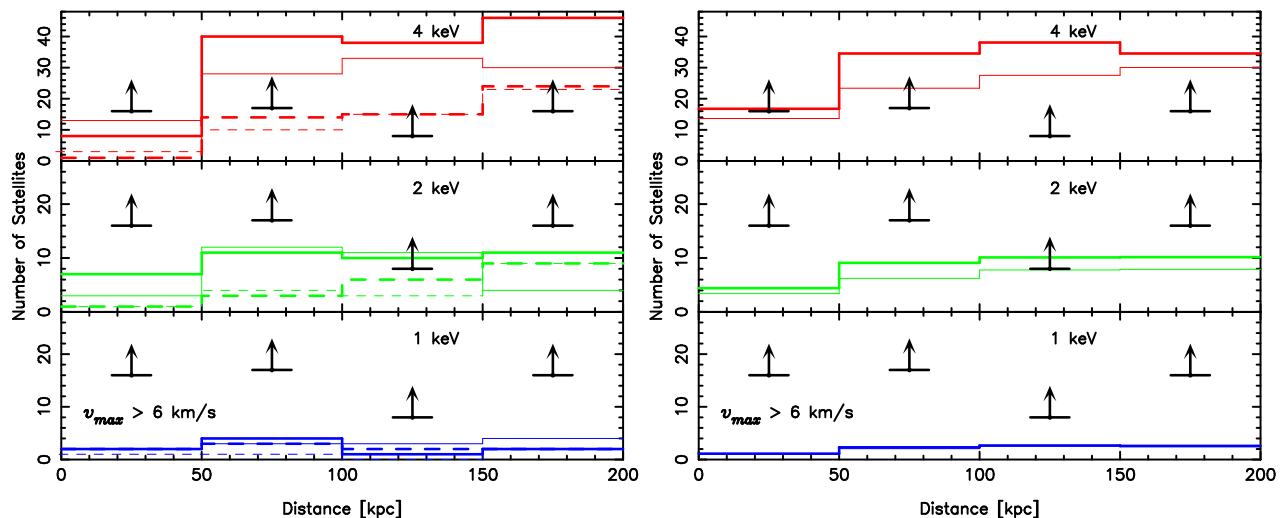


FIG. 10. (*left*) Number of satellites with distance from the Milky Way grouped into 50 kpc bins. The simulation satellites have been cut by circular velocity > 6 km/s. Solid lines show the data from the high resolution and dashed lines show the low resolution simulations, thick lines are the *set B* simulations. The bars with arrows are the observed satellites after correcting for the sky coverage of the SDSS but not including Willman 1. Observations are incomplete at distances greater than about 50 – 100 kpc (depending on the luminosity and surface brightness of the dwarf), while simulations have not converged for less than about 100 kpc for high resolution and 150 kpc for low resolution. (*right*) Number of satellites with distance from the Milky Way like the plot at left but calculated from the convergence equation [Eq. 12]. The convergence correction affects mainly the 4 keV 0 – 50 kpc bin.

lites due to partial sky coverage and on the number of simulated satellites due to Poisson and intrinsic scatter, that partially reflects observational uncertainties on the mass and v_{max} of the Milky Way, we find much weaker lower limits on m_{wdm} than 4 keV. In the future however, the lower limit on m_{wdm} will improve as observations of MW satellites become more complete. The scatter of the simulation can also be reduced using constrained simulations of the Local Group (also including the effect of baryons) in combination with more accurate determination of the mass, rotation curve, and concentration of the Milky Way.

Considering the various uncertainties in the number of observed and simulated satellites, we found a conservative lower limit of $m_{WDM} > 2.3$ keV (2σ) on the dark matter particle mass. We also found the 1 keV WDM simulations have too few satellites to match the Milky Way observations. This agrees with the semianalytic modeling and Milky Way satellite luminosity functions in WDM cosmologies work of Macciò and Fontanot [14]; however, we only apply a cut to the simulated halos to avoid numerical effects and do not make assumptions on how the dark matter halos are populated by luminous galaxies.

Our result can also be compared to limits on the particle mass from the Lyman- α forest in high redshift quasars. Lyman- α absorption by neutral hydrogen along the line of sight to distant quasars over redshifts 2–6 probes the matter power spectrum in the mildly nonlinear regime on scales 1–80 Mpc/ h . Viel et al. [52, 109, 110] have numerically modeled the Lyman- α forest flux power

spectra for varied cosmological parameters and compared to observed quasar forests to obtain lower limits on the dark matter particle mass. Their 2006 work [109] used low resolution spectra for 3035 quasars ($2.2 < z < 4.2$) from the SDSS [111] and found a 2σ lower limit of 2 keV for a thermal WDM particle. This limit agrees with our results that a 2.3 keV particle is the lower limit that can reproduce the observed number of Milky Way satellites and agrees with the Lyman- α work of Seljak et al. [112] who find a 2σ limit > 2.5 keV for a thermal particle. The latest work of Viel et al. [110] uses high resolution spectra for 55 quasars ($2.0 < z < 6.4$) from the Keck HIRES spectrograph in addition to the SDSS quasars. With the new data they report a lower limit of 4 keV (2σ). A caveat arises in Viel et al. [113], who show the flux power spectrum from the SDSS data prefer larger values of the intergalactic medium (IGM) temperature at mean density than expected from photoionization. The flux power spectrum temperature is also higher than that derived from an analysis of the flux probability distribution function of 18 high resolution spectra from the Very Large Telescope and also higher than constraints from the widths of thermally broadened absorption lines [114, 115]. This could be explained by an unaccounted for systematic error in the SDSS flux power spectrum data which may also affect the derived dark matter particle mass limits.

Using the scaling relation for sterile neutrinos we find a lower limit $m_s > 13.3$ keV with 95% confidence for a DW produced sterile neutrino particle. Scaling to the other production mechanisms we get $m_s > 8.9$ keV for the SF

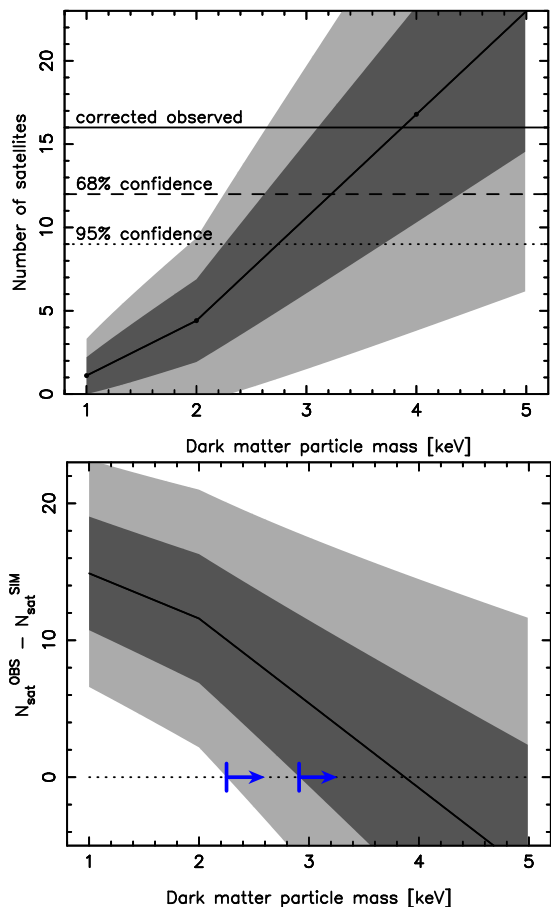


FIG. 11. *top* Number of satellites from 0-50 kpc calculated from the convergence equation in the *set B* high resolution simulation for $v_{max} > 6$ km/s (sloped solid line) with 1σ and 2σ limits (shaded regions) compared to the observed number of Milky Way satellites, excluding Willman 1, with correction for sky coverage (solid horizontal line) and at 68% and 95% confidence (dashed and dotted horizontal lines). *bottom* The observed number of satellites minus the number of satellites in simulation with 1σ and 2σ limits (shaded regions). The number of satellites in simulation must be greater than or equal to the number of observed satellites, therefore where this quantity equals zero sets a lower limit to the dark matter particle mass (arrows).

mechanism and $m_s > 3.0$ keV for Higgs decay sterile neutrinos; however, we note this is not based on transfer function calculations for the SF and Higgs mechanisms but assumes a simple scaling for the average momentum for the different production mechanisms [34]. The Lyman- α forest observations discussed above in the context of a thermal particle also set limits on the sterile neutrino mass. The 2006 work of Viel et al. [109] sets $m_s > 11$ keV and is similar to the Seljak et al. [112] limit $m_s > 14$ keV. The 2008 work of Viel et al. [110] sets the highest limit of $m_s > 28$ keV but is subject to the caveats mentioned above.

Sterile neutrinos are expected to radiatively decay to a lighter mass neutrino and a X-ray photon with en-

ergy $E_\gamma = m_s/2$. X-ray observations of the diffuse X-ray background [116] and dark matter halos in clusters [117–120], M31 [121], dwarf spheroidal galaxies [122–125], and the halo of the Milky Way [122, 126, 127] have all been used to set constraints on the sterile neutrino mass. Observations of the diffuse X-ray background have set $m_s < 9.3$ keV [116], while the Virgo and Coma clusters have been used to set $m_s < 6.3$ keV [117] which also agrees with limits from the bullet cluster, 1E 0657-56, $m_s < 6.3$ keV [120] and is close to results from the Milky Way halo $m_s < 5.7$ keV [127]. Tighter constraints have been determined from M31 observations $m_s < 3.5$ keV [121] and from the dwarf spheroidal Ursa Minor $m_s < 2.5$ keV [125].

These upper limits are well below the lower limits derived in this work and from Lyman- α observations and seem to rule out the DW and SF production mechanisms. However, all of these mass limits, including the constraints set in this work, are model dependent and make certain assumptions. In general X-ray constraints depend on the sterile neutrino mass, the mixing angle with active neutrinos θ , and the cosmic matter density of sterile neutrinos Ω_s . There are also assumptions about the initial conditions, that there were no sterile neutrinos in the early Universe at temperatures > 1 GeV, there was no entropy dilution after creation, and no coupling to other particles. There are also uncertainties with the calculation of production rates because these occur at temperatures where the plasma is neither well described by hadronic nor quark models [116, 128]. Depending on the assumptions made and the adopted production model the relationship between m_s , θ , and Ω_s changes so that robust constraints cannot be placed on any one model parameter.

There has also been a report of a detection of a dark matter X-ray emission line from Willman 1 consistent with $m_s = 5.0 \pm 0.2$ keV [105, 106]. This detection is provisional [107] but if confirmed the limits derived in this work imply the sterile neutrinos are not produced by the DW mechanism or do not constitute the entirety of the dark matter.

V. SUMMARY

We conducted N -body simulations of the formation of a MW-sized dark matter halo in CDM and WDM cosmologies. Such simulations are complicated by the formation of nonphysical small mass halos due to the discreteness of the initial conditions but with sufficient resolution they are only important at small scales and can be avoided with an appropriate circular velocity cut.

We studied the number of satellite halos as a function of distance from the MW. The 4 keV WDM simulation can adequately reproduce the observed number of satellites at hundreds of kiloparsecs while the 2 keV simulation is slightly deficient and the 1 keV severely deficient. Our high resolution simulations followed the for-

mation of two MW-sized halos. Numerical simulations of MW-sized halos show significant variance in the number of satellites, an effect that can be easily quantified using published studies and was incorporated in our results. We calculated the number of satellites in the inner 50 kpc, corrected for the effects of numerical destruction, and accounted for the variance by conservatively adopting a 30% (1σ) intrinsic scatter in the number of satellites in addition to a scatter from Poisson statistics. We also accounted for the uncertainty in the number of observed MW satellites due to the survey area of the SDSS and derived a very conservative lower limit on the dark matter particle mass of > 2.3 keV (95% C.L.). This agrees with the earlier Lyman- α forest modeling work of Viel et al. [109] that $m_{WDM} > 2$ keV but the two methods are independent and almost certainly are subject to different systematic errors if any exist. Their latest work [110] raised the limit to $m_{WDM} > 4$ keV but problems with the derived IGM temperature and mean density may indicate the SDSS spectra they used may suffer a systematic error [113].

Our lower limit of 2.3 keV for a thermal dark matter particle scales to lower limits of 13.3, 8.9, 3.0 keV (95% C.L.) for DW, SF, and Higgs decay produced sterile neutrinos. Sterile neutrinos, if they exist, are expected to decay into X-rays and active neutrinos. Observations of the unresolved cosmic X-ray background and X-ray observations of dark matter halos on scales from dwarf galaxies to clusters set upper limits below our lower limit and the limits of Lyman- α forest modeling. These limits are derived under many assumptions and, in general, the constraints apply to a parameter space of m_s , θ , and Ω_s .

Our constraint is a conservative lower limit since we only correct the number of SDSS dwarfs for sky completeness. An analysis that takes into account the surface brightness limits of the observational data may allow tighter constraints; however, the analysis would be somewhat model dependent. We have also not included the ef-

fects on subhalos of baryonic structures in the inner MW halo such as a disk. The presence of a disk could lead to greater subhalo destruction due to increased dynamical friction and tidal heating. By increasing the subhalo destruction rate in the inner halo, disks would increase our lower bounds on the dark matter particle mass. The assumption of no disk is a conservative one and an analysis that includes a disk may allow tighter constraints.

We have demonstrated how N -body simulations of the MW and its satellites can set limits on the dark matter particle mass comparable to and independent of complementary methods such as modeling the Lyman- α forest. These limits are helped greatly by the discovery of many new MW satellites in the SDSS. There may still be a population of low luminosity, low surface brightness dwarf galaxies undetectable by the SDSS [100–103]. Future surveys like LSST, DES, PanSTARRS, and SkyMapper have the potential to discover many more MW satellites and further improve constraints on the mass of the dark matter particle. Better constraints will result from the smaller uncertainty in the number of observed satellites achieved by improving the sky coverage and reducing luminosity corrections. In addition, the existence of a yet unknown population of even fainter satellites is not unlikely.

ACKNOWLEDGMENTS

It is our pleasure to thank Alexander Kusenko, Kev Abazajian, Signe Riemer-Sørensen, Oleg Ruchayskiy, Maxim Khlopov, H. J. de Vega, N. G. Sanchez, and Salucci Paolo for helpful discussions, comments, and suggestions. Emil Polisensky acknowledges support under the Edison Memorial Graduate Training Program at the Naval Research Laboratory.

-
- [1] A. Klypin, A. V. Kravtsov, O. Valenzuela, and F. Prada, *Astrophys. J.* **522**, 82 (Sep. 1999), arXiv:astro-ph/9901240.
 - [2] B. Moore, S. Ghigna, F. Governato, G. Lake, T. Quinn, J. Stadel, and P. Tozzi, *Astrophys. J. Lett.* **524**, L19 (Oct. 1999), arXiv:astro-ph/9907411.
 - [3] G. Efstathiou, *Mon. Not. R. Astron. Soc.* **256**, 43P (May 1992).
 - [4] A. A. Thoul and D. H. Weinberg, *Astrophys. J.* **465**, 608 (Jul. 1996), arXiv:astro-ph/9510154.
 - [5] J. S. Bullock, A. V. Kravtsov, and D. H. Weinberg, *Astrophys. J.* **548**, 33 (Feb. 2001), arXiv:astro-ph/0007295.
 - [6] M. Ricotti and J. P. Ostriker, *Mon. Not. R. Astron. Soc.* **352**, 547 (Aug. 2004), arXiv:astro-ph/0311003.
 - [7] M. Ricotti, J. P. Ostriker, and N. Y. Gnedin, *Mon. Not. R. Astron. Soc.* **357**, 207 (Feb. 2005), arXiv:astro-ph/0404318.
 - [8] P. Colín, V. Avila-Reese, and O. Valenzuela, *Astrophys. J.* **542**, 622 (Oct. 2000), arXiv:astro-ph/0004115.
 - [9] V. Avila-Reese, P. Colín, O. Valenzuela, E. D’Onghia, and C. Firmani, *Astrophys. J.* **559**, 516 (Oct. 2001), arXiv:astro-ph/0010525.
 - [10] P. Bode, J. P. Ostriker, and N. Turok, *Astrophys. J.* **556**, 93 (Jul. 2001), arXiv:astro-ph/0010389.
 - [11] A. Knebe, J. E. G. Devriendt, A. Mahmood, and J. Silk, *Mon. Not. R. Astron. Soc.* **329**, 813 (Feb. 2002), arXiv:astro-ph/0105316.
 - [12] A. Knebe, J. E. G. Devriendt, B. K. Gibson, and J. Silk, *Mon. Not. R. Astron. Soc.* **345**, 1285 (Nov. 2003), arXiv:astro-ph/0302443.
 - [13] A. R. Zentner and J. S. Bullock, *Astrophys. J.* **598**, 49 (Nov. 2003), arXiv:astro-ph/0304292.
 - [14] A. V. Maccio’ and F. Fontanot, ArXiv e-prints (Oct.

- 2009), arXiv:0910.2460.
- [15] F. C. van den Bosch and R. A. Swaters, *Mon. Not. R. Astron. Soc.* **325**, 1017 (Aug. 2001), arXiv:astro-ph/0006048.
- [16] R. A. Swaters, B. F. Madore, F. C. van den Bosch, and M. Balcells, *Astrophys. J.* **583**, 732 (Feb. 2003), arXiv:astro-ph/0210152.
- [17] D. T. F. Weldrake, W. J. G. de Blok, and F. Walter, *Mon. Not. R. Astron. Soc.* **340**, 12 (Mar. 2003), arXiv:astro-ph/0210568.
- [18] F. Donato, G. Gentile, and P. Salucci, *Mon. Not. R. Astron. Soc.* **353**, L17 (Sep. 2004), arXiv:astro-ph/0403206.
- [19] G. Gentile, A. Burkert, P. Salucci, U. Klein, and F. Walter, *Astrophys. J. Lett.* **634**, L145 (Dec. 2005), arXiv:astro-ph/0506538.
- [20] J. D. Simon, A. D. Bolatto, A. Leroy, L. Blitz, and E. L. Gates, *Astrophys. J.* **621**, 757 (Mar. 2005), arXiv:astro-ph/0412035.
- [21] G. Gentile, P. Salucci, U. Klein, and G. L. Granato, *Mon. Not. R. Astron. Soc.* **375**, 199 (Feb. 2007), arXiv:astro-ph/0611355.
- [22] P. Salucci, A. Lapi, C. Tonini, G. Gentile, I. Yegorova, and U. Klein, *Mon. Not. R. Astron. Soc.* **378**, 41 (Jun. 2007), arXiv:astro-ph/0703115.
- [23] R. Kuzio de Naray, G. D. Martinez, J. S. Bullock, and M. Kaplinghat, *Astrophys. J. Lett.* **710**, L161 (Feb. 2010), arXiv:0912.3518 [astro-ph.CO].
- [24] A. L. Melott, ArXiv e-prints (Sep. 2007), arXiv:0709.0745.
- [25] J. Wang and S. D. M. White, *Mon. Not. R. Astron. Soc.* **380**, 93 (Sep. 2007), arXiv:astro-ph/0702575.
- [26] F. J. Castander, *Astrophys. Space Sci.* **263**, 91 (Jun. 1998).
- [27] V. Springel, *Mon. Not. R. Astron. Soc.* **364**, 1105 (Dec. 2005), arXiv:astro-ph/0505010.
- [28] D. N. Spergel, R. Bean, O. Doré, M. R. Nolta, C. L. Bennett, J. Dunkley, G. Hinshaw, N. Jarosik, E. Komatsu, L. Page, H. V. Peiris, L. Verde, M. Halpern, R. S. Hill, A. Kogut, M. Limon, S. S. Meyer, N. Odegaard, G. S. Tucker, J. L. Weiland, E. Wollack, and E. L. Wright, *Astrophys. J. Suppl.* **170**, 377 (Jun. 2007), arXiv:astro-ph/0603449.
- [29] J. Diemand, M. Kuhlen, P. Madau, M. Zemp, B. Moore, D. Potter, and J. Stadel, *Nature (London)* **454**, 735 (Aug. 2008), arXiv:0805.1244.
- [30] E. Bertschinger, *Astrophys. J. Suppl.* **137**, 1 (Nov. 2001), arXiv:astro-ph/0103301.
- [31] J. M. Bardeen, J. R. Bond, N. Kaiser, and A. S. Szalay, *Astrophys. J.* **304**, 15 (May 1986).
- [32] D. J. Eisenstein and W. Hu, *Astrophys. J.* **496**, 605 (Mar. 1998), arXiv:astro-ph/9709112.
- [33] D. Gorbunov, A. Khmel'nitsky, and V. Rubakov, *Journal of High Energy Physics* **12**, 55 (Dec. 2008), arXiv:0805.2836 [hep-ph].
- [34] A. Kusenko, *Physics Reports* **481**, 1 (Sep. 2009), arXiv:0906.2968.
- [35] S. Gninenko, ArXiv e-prints (Sep. 2010), arXiv:1009.5536 [hep-ph].
- [36] S. N. Gninenko and D. S. Gorbunov, *Phys. Rev. D* **81**, 075013 (Apr. 2010), arXiv:0907.4666 [hep-ph].
- [37] G. Karagiorgi, Z. Djurcic, J. M. Conrad, M. H. Shaevitz, and M. Sorel, *Phys. Rev. D* **80**, 073001 (Oct. 2009), arXiv:0906.1997 [hep-ph].
- [38] M. Sorel, J. M. Conrad, and M. H. Shaevitz, *Phys. Rev. D* **70**, 073004 (Oct. 2004), arXiv:hep-ph/0305255.
- [39] A. Melchiorri, O. Mena, S. Palomares-Ruiz, S. Pascoli, A. Slosar, and M. Sorel, *J. Cosmo. and Astropart. Phys.* **1**, 36 (Jan. 2009), arXiv:0810.5133 [hep-ph].
- [40] M. Maltoni and T. Schwetz, *Phys. Rev. D* **76**, 093005 (Nov. 2007), arXiv:0705.0107 [hep-ph].
- [41] H. Päs, S. Pakvasa, and T. J. Weiler, *Phys. Rev. D* **72**, 095017 (Nov. 2005), arXiv:hep-ph/0504096.
- [42] E. Akhmedov and T. Schwetz, *Journal of High Energy Physics* **10**, 115 (Oct. 2010), arXiv:1007.4171 [hep-ph].
- [43] C. Athanassopoulos, L. B. Auerbach, D. A. Bauer, R. D. Bolton, B. Boyd, R. L. Burman, D. O. Caldwell, I. Cohen, B. D. Dieterle, J. B. Donahue, A. M. Eisner, A. Fazely, F. J. Federspiel, G. T. Garvey, M. Gray, and et al., *Physical Review Letters* **75**, 2650 (Oct. 1995), arXiv:nucl-ex/9504002.
- [44] C. Athanassopoulos, L. B. Auerbach, R. L. Burman, I. Cohen, D. O. Caldwell, B. D. Dieterle, J. B. Donahue, A. M. Eisner, A. Fazely, F. J. Federspiel, G. T. Garvey, M. Gray, R. M. Gunasingha, R. Imlay, K. Johnston, H. J. Kim, W. C. Louis, R. Majkic, J. Margulies, K. McIlhany, W. Metcalf, G. B. Mills, R. A. Reeder, V. Sandberg, D. Smith, I. Stancu, W. Strossman, R. Tayloe, G. J. Vandalen, W. Vernon, N. Wadia, J. Waltz, Y. Wang, D. H. White, D. Works, Y. Xiao, and S. Yellin, *Physical Review Letters* **77**, 3082 (Oct. 1996), arXiv:nucl-ex/9605003.
- [45] C. Athanassopoulos, L. B. Auerbach, R. L. Burman, D. O. Caldwell, E. D. Church, I. Cohen, J. B. Donahue, A. Fazely, F. J. Federspiel, G. T. Garvey, R. M. Gunasingha, R. Imlay, K. Johnston, H. J. Kim, W. C. Louis, R. Majkic, K. McIlhany, G. B. Mills, R. A. Reeder, V. Sandberg, D. Smith, I. Stancu, W. Strossman, R. Tayloe, G. J. Vandalen, W. Vernon, N. Wadia, J. Waltz, D. H. White, D. Works, Y. Xiao, and S. Yellin, *Physical Review Letters* **81**, 1774 (Aug. 1998), arXiv:nucl-ex/9709006.
- [46] C. Athanassopoulos, L. B. Auerbach, R. L. Burman, D. O. Caldwell, E. D. Church, I. Cohen, J. B. Donahue, A. Fazely, F. J. Federspiel, G. T. Garvey, R. M. Gunasingha, R. Imlay, K. Johnston, H. J. Kim, W. C. Louis, R. Majkic, K. McIlhany, W. Metcalf, G. B. Mills, R. A. Reeder, V. Sandberg, D. Smith, I. Stancu, W. Strossman, R. Tayloe, G. J. Vandalen, W. Vernon, N. Wadia, J. Waltz, D. H. White, D. Works, Y. Xiao, and S. Yellin, *Phys. Rev. C* **58**, 2489 (Oct. 1998), arXiv:nucl-ex/9706006.
- [47] A. A. Aguilar-Arevalo, A. O. Bazarko, S. J. Brice, B. C. Brown, L. Bugel, J. Cao, L. Coney, J. M. Conrad, D. C. Cox, A. Curioni, Z. Djurcic, D. A. Finley, B. T. Fleming, R. Ford, F. G. Garcia, G. T. Garvey, C. Green, J. A. Green, T. L. Hart, E. Hawker, R. Imlay, R. A. Johnson, P. Kasper, T. Katori, T. Kobilarcik, I. Kourbanis, S. Koutsoliotas, E. M. Laird, J. M. Link, Y. Liu, Y. Liu, W. C. Louis, K. B. M. Mahn, W. Marsh, P. S. Martin, G. McGregor, W. Metcalf, P. D. Meyers, F. Mills, G. B. Mills, J. Monroe, C. D. Moore, R. H. Nelson, P. Nienaber, S. Ouedraogo, R. B. Patterson, D. Perevalov, C. C. Polly, E. Prebys, J. L. Raaf, H. Ray, B. P. Roe, A. D. Russell, V. Sandberg, R. Schi-

- rato, D. Schmitz, M. H. Shaevitz, F. C. Shoemaker, D. Smith, M. Sorel, P. Spentzouris, I. Stancu, R. J. Stefanski, M. Sung, H. A. Tanaka, R. Tayloe, M. Tzanov, R. van de Water, M. O. Wascko, D. H. White, M. J. Wilking, H. J. Yang, G. P. Zeller, and E. D. Zimmerman, *Physical Review Letters* **98**, 231801 (Jun. 2007), arXiv:0704.1500 [hep-ex].
- [48] A. A. Aguilar-Arevalo, C. E. Anderson, A. O. Bazarko, S. J. Brice, B. C. Brown, L. Bugel, J. Cao, L. Coney, J. M. Conrad, D. C. Cox, A. Curioni, Z. Djurcic, D. A. Finley, B. T. Fleming, R. Ford, F. G. Garcia, G. T. Garvey, C. Green, J. A. Green, T. L. Hart, E. Hawker, R. Imlay, R. A. Johnson, G. Karagiorgi, P. Kasper, T. Katori, T. Kobilarcik, I. Kourbanis, S. Koutsoliotas, E. M. Laird, S. K. Linden, J. M. Link, Y. Liu, Y. Liu, W. C. Louis, K. B. M. Mahn, W. Marsh, G. McGregor, W. Metcalf, P. D. Meyers, F. Mills, G. B. Mills, J. Monroe, C. D. Moore, R. H. Nelson, V. T. Nguyen, P. Nienaber, J. A. Nowak, S. Ouedraogo, R. B. Patterson, D. Perevalov, C. C. Polly, E. Prebys, J. L. Raaf, H. Ray, B. P. Roe, A. D. Russell, V. Sandberg, R. Schirato, D. Schmitz, M. H. Shaevitz, F. C. Shoemaker, D. Smith, M. Sodeberg, M. Sorel, P. Spentzouris, I. Stancu, R. J. Stefanski, M. Sung, H. A. Tanaka, R. Tayloe, M. Tzanov, R. van de Water, M. O. Wascko, D. H. White, M. J. Wilking, H. J. Yang, G. P. Zeller, and E. D. Zimmerman, *Physical Review Letters* **102**, 101802 (Mar. 2009), arXiv:0812.2243 [hep-ex].
- [49] A. A. Aguilar-Arevalo, C. E. Anderson, S. J. Brice, B. C. Brown, L. Bugel, J. M. Conrad, R. Dharmapalan, Z. Djurcic, B. T. Fleming, R. Ford, F. G. Garcia, G. T. Garvey, J. Mirabal, J. Grange, J. A. Green, R. Imlay, R. A. Johnson, G. Karagiorgi, T. Katori, T. Kobilarcik, S. K. Linden, W. C. Louis, K. B. M. Mahn, W. Marsh, C. Mauger, W. Metcalf, G. B. Mills, C. D. Moore, J. Mousseau, R. H. Nelson, V. Nguyen, P. Nienaber, J. A. Nowak, B. Osmanov, Z. Pavlovic, D. Perevalov, C. C. Polly, H. Ray, B. P. Roe, A. D. Russell, R. Schirato, M. H. Shaevitz, M. Sorel, J. Spitz, I. Stancu, R. J. Stefanski, R. Tayloe, M. Tzanov, R. G. van de Water, M. O. Wascko, D. H. White, M. J. Wilking, G. P. Zeller, and E. D. Zimmerman, *Physical Review Letters* **105**, 181801 (Oct. 2010).
- [50] S. Dodelson and L. M. Widrow, *Physical Review Letters* **72**, 17 (Jan. 1994), arXiv:hep-ph/9303287.
- [51] K. Abazajian, *Phys. Rev. D* **73**, 063513 (Mar. 2006), arXiv:astro-ph/0512631.
- [52] M. Viel, J. Lesgourgues, M. G. Haehnelt, S. Matarrese, and A. Riotto, *Phys. Rev. D* **71**, 063534 (Mar. 2005), arXiv:astro-ph/0501562.
- [53] X. Shi and G. M. Fuller, *Physical Review Letters* **82**, 2832 (Apr. 1999), arXiv:astro-ph/9810076.
- [54] A. Kusenko, *Physical Review Letters* **97**, 241301 (Dec. 2006), arXiv:hep-ph/0609081.
- [55] M. Kamionkowski and A. R. Liddle, *Physical Review Letters* **84**, 4525 (May 2000), arXiv:astro-ph/9911103.
- [56] K. Sigurdson and M. Kamionkowski, *Physical Review Letters* **92**, 171302 (Apr. 2004), arXiv:astro-ph/0311486.
- [57] M. Kaplinghat, *Phys. Rev. D* **72**, 063510 (Sep. 2005), arXiv:astro-ph/0507300.
- [58] M. Y. Khlopov, *ArXiv Astrophysics e-prints*(Nov. 2005), arXiv:astro-ph/0511796.
- [59] M. Y. Khlopov, *ArXiv Astrophysics e-prints*(Jul. 2006), arXiv:astro-ph/0607048.
- [60] K. Belotsky, M. Khlopov, and K. Shibaev, in *Particle Physics at the Year of 250th Anniversary of Moscow University*, edited by A. Studenikin (2006) pp. 180–+, arXiv:astro-ph/0602261.
- [61] K. M. Belotsky, M. Y. Khlopov, and K. I. Shibaev, *Gravitation and Cosmology* **12**, 93 (Jun. 2006), arXiv:astro-ph/0604518.
- [62] M. Y. Khlopov and C. Kouvaris, *Phys. Rev. D* **77**, 065002 (Mar. 2008), arXiv:0710.2189.
- [63] M. Y. Khlopov and C. Kouvaris, *Phys. Rev. D* **78**, 065040 (Sep. 2008), arXiv:0806.1191.
- [64] M. Y. Khlopov, *ArXiv e-prints*(Jun. 2008), arXiv:0806.3581.
- [65] D. J. Eisenstein and P. Hut, *Astrophys. J.* **498**, 137 (May 1998), arXiv:astro-ph/9712200.
- [66] S. R. Knollmann and A. Knebe, *Astrophys. J. Suppl.* **182**, 608 (Jun. 2009), arXiv:0904.3662.
- [67] V. R. Eke, S. Cole, and C. S. Frenk, *Mon. Not. R. Astron. Soc.* **282**, 263 (Sep. 1996), arXiv:astro-ph/9601088.
- [68] G. L. Bryan and M. L. Norman, *Astrophys. J.* **495**, 80 (Mar. 1998), arXiv:astro-ph/9710107.
- [69] C. Power, J. F. Navarro, A. Jenkins, C. S. Frenk, S. D. M. White, V. Springel, J. Stadel, and T. Quinn, *Mon. Not. R. Astron. Soc.* **338**, 14 (Jan. 2003), arXiv:astro-ph/0201544.
- [70] S. Ghigna, B. Moore, F. Governato, G. Lake, T. Quinn, and J. Stadel, *Astrophys. J.* **544**, 616 (Dec. 2000), arXiv:astro-ph/9910166.
- [71] A. Helmi, S. D. White, and V. Springel, *Phys. Rev. D* **66**, 063502 (Sep. 2002), arXiv:astro-ph/0201289.
- [72] L. Gao, S. D. M. White, A. Jenkins, F. Stoehr, and V. Springel, *Mon. Not. R. Astron. Soc.* **355**, 819 (Dec. 2004), arXiv:astro-ph/0404589.
- [73] G. De Lucia, G. Kauffmann, V. Springel, S. D. M. White, B. Lanzoni, F. Stoehr, G. Tormen, and N. Yoshida, *Mon. Not. R. Astron. Soc.* **348**, 333 (Feb. 2004), arXiv:astro-ph/0306205.
- [74] F. C. van den Bosch, G. Tormen, and C. Giocoli, *Mon. Not. R. Astron. Soc.* **359**, 1029 (May 2005), arXiv:astro-ph/0409201.
- [75] J. Diemand, M. Kuhlen, and P. Madau, *Astrophys. J.* **657**, 262 (Mar. 2007), arXiv:astro-ph/0611370.
- [76] C. Giocoli, G. Tormen, and F. C. van den Bosch, *Mon. Not. R. Astron. Soc.* **386**, 2135 (Jun. 2008), arXiv:0712.1563.
- [77] V. Springel, J. Wang, M. Vogelsberger, A. Ludlow, A. Jenkins, A. Helmi, J. F. Navarro, C. S. Frenk, and S. D. M. White, *Mon. Not. R. Astron. Soc.* **391**, 1685 (Dec. 2008), arXiv:0809.0898.
- [78] T. Ishiyama, T. Fukushige, and J. Makino, *Astrophys. J.* **696**, 2115 (May 2009), arXiv:0812.0683.
- [79] A. Klypin, S. Trujillo-Gomez, and J. Primack, *ArXiv e-prints*(Feb. 2010), arXiv:1002.3660 [astro-ph.CO].
- [80] N. Jarosik, C. L. Bennett, J. Dunkley, B. Gold, M. R. Greason, M. Halpern, R. S. Hill, G. Hinshaw, A. Kogut, E. Komatsu, D. Larson, M. Limon, S. S. Meyer, M. R.olta, N. Odegard, L. Page, K. M. Smith, D. N. Spergel, G. S. Tucker, J. L. Weiland, E. Wollack, and E. L. Wright, *ArXiv e-prints*(Jan. 2010),

- arXiv:1001.4744 [astro-ph.CO].
- [81] R. Barkana, Z. Haiman, and J. P. Ostriker, *Astrophys. J.* **558**, 482 (Sep. 2001), arXiv:astro-ph/0102304.
- [82] S. M. Walsh, B. Willman, and H. Jerjen, *Astron. J.* **137**, 450 (Jan. 2009), arXiv:0807.3345.
- [83] E. J. Tollerud, J. S. Bullock, L. E. Strigari, and B. Willman, *Astrophys. J.* **688**, 277 (Nov. 2008), arXiv:0806.4381.
- [84] S. Kopolov, V. Belokurov, N. W. Evans, P. C. Hewett, M. J. Irwin, G. Gilmore, D. B. Zucker, H. Rix, M. Fellhauer, E. F. Bell, and E. V. Glushkova, *Astrophys. J.* **686**, 279 (Oct. 2008), arXiv:0706.2687.
- [85] M. L. Mateo, *Ann. Rev. Astron. Astrophys.* **36**, 435 (1998), arXiv:astro-ph/9810070.
- [86] M. Geha, B. Willman, J. D. Simon, L. E. Strigari, E. N. Kirby, D. R. Law, and J. Strader, *Astrophys. J.* **692**, 1464 (Feb. 2009), arXiv:0809.2781.
- [87] N. F. Martin, R. A. Ibata, S. C. Chapman, M. Irwin, and G. F. Lewis, *Mon. Not. R. Astron. Soc.* **380**, 281 (Sep. 2007), arXiv:0705.4622.
- [88] J. D. Simon and M. Geha, *Astrophys. J.* **670**, 313 (Nov. 2007), arXiv:0706.0516.
- [89] V. Belokurov, M. G. Walker, N. W. Evans, G. Gilmore, M. J. Irwin, M. Mateo, L. Mayer, E. Olszewski, J. Bechtold, and T. Pickering, *Mon. Not. R. Astron. Soc.* **397**, 1748 (Aug. 2009), arXiv:0903.0818.
- [90] B. Willman, M. R. Blanton, A. A. West, J. J. Dalcanton, D. W. Hogg, D. P. Schneider, N. Wherry, B. Yanny, and J. Brinkmann, *Astron. J.* **129**, 2692 (Jun. 2005), arXiv:astro-ph/0410416.
- [91] V. Belokurov, D. B. Zucker, N. W. Evans, J. T. Kleyna, S. Kopolov, S. T. Hodgkin, M. J. Irwin, G. Gilmore, M. I. Wilkinson, M. Fellhauer, D. M. Bramich, P. C. Hewett, S. Vidrih, J. T. A. De Jong, J. A. Smith, H. Rix, E. F. Bell, R. F. G. Wyse, H. J. Newberg, P. A. Mayeur, B. Yanny, C. M. Rockosi, O. Y. Gnedin, D. P. Schneider, T. C. Beers, J. C. Barentine, H. Brewington, J. Brinkmann, M. Harvanek, S. J. Kleinman, J. Krzesinski, D. Long, A. Nitta, and S. A. Snedden, *Astrophys. J.* **654**, 897 (Jan. 2007), arXiv:astro-ph/0608448.
- [92] S. M. Walsh, H. Jerjen, and B. Willman, *Astrophys. J. Lett.* **662**, L83 (Jun. 2007), arXiv:0705.1378.
- [93] L. L. Watkins, N. W. Evans, V. Belokurov, M. C. Smith, P. C. Hewett, D. M. Bramich, G. F. Gilmore, M. J. Irwin, S. Vidrih, L. Wyrzykowski, and D. B. Zucker, *Mon. Not. R. Astron. Soc.* **398**, 1757 (Oct. 2009), arXiv:0906.0498.
- [94] J. A. Kollmeier, A. Gould, S. Shectman, I. B. Thompson, G. W. Preston, J. D. Simon, J. D. Crane, Ž. Ivezić, and B. Sesar, *Astrophys. J. Lett.* **705**, L158 (Nov. 2009), arXiv:0908.1381.
- [95] J. T. A. de Jong, N. F. Martin, H. Rix, K. W. Smith, S. Jin, and A. V. Maccio', *ArXiv e-prints*(Dec. 2009), arXiv:0912.3251.
- [96] V. Belokurov, M. G. Walker, N. W. Evans, D. C. Faria, G. Gilmore, M. J. Irwin, S. Kopolov, M. Mateo, E. Olszewski, and D. B. Zucker, *Astrophys. J. Lett.* **686**, L83 (Oct. 2008), arXiv:0807.2831.
- [97] V. Belokurov, M. G. Walker, N. W. Evans, G. Gilmore, M. J. Irwin, D. Just, S. Kopolov, M. Mateo, E. Olszewski, L. Watkins, and L. Wyrzykowski, *Astrophys. J. Lett.* **712**, L103 (Mar. 2010), arXiv:1002.0504.
- [98] D. B. Zucker, V. Belokurov, N. W. Evans, M. I. Wilkinson, M. J. Irwin, T. Sivarani, S. Hodgkin, D. M. Bramich, J. M. Irwin, G. Gilmore, B. Willman, S. Vidrih, M. Fellhauer, P. C. Hewett, T. C. Beers, E. F. Bell, E. K. Grebel, D. P. Schneider, H. J. Newberg, R. F. G. Wyse, C. M. Rockosi, B. Yanny, R. Lupton, J. A. Smith, J. C. Barentine, H. Brewington, J. Brinkmann, M. Harvanek, S. J. Kleinman, J. Krzesinski, D. Long, A. Nitta, and S. A. Snedden, *Astrophys. J. Lett.* **643**, L103 (Jun. 2006), arXiv:astro-ph/0604354.
- [99] M. J. Irwin, V. Belokurov, N. W. Evans, E. V. Ryan-Weber, J. T. A. de Jong, S. Kopolov, D. B. Zucker, S. T. Hodgkin, G. Gilmore, P. Prema, L. Hebb, A. Begum, M. Fellhauer, P. C. Hewett, R. C. Kennicutt, Jr., M. I. Wilkinson, D. M. Bramich, S. Vidrih, H. Rix, T. C. Beers, J. C. Barentine, H. Brewington, M. Harvanek, J. Krzesinski, D. Long, A. Nitta, and S. A. Snedden, *Astrophys. J. Lett.* **656**, L13 (Feb. 2007), arXiv:astro-ph/0701154.
- [100] M. Ricotti and N. Y. Gnedin, *Astrophys. J.* **629**, 259 (Aug. 2005), arXiv:astro-ph/0408563.
- [101] M. Ricotti, N. Y. Gnedin, and J. M. Shull, *Astrophys. J.* **685**, 21 (Sep. 2008), arXiv:0802.2715.
- [102] M. Ricotti, *Advances in Astronomy* **2010** (2010), doi: "bibinfo doi 10.1155/2010/271592, arXiv:0911.2792.
- [103] M. S. Bovill and M. Ricotti, *Astrophys. J.* **693**, 1859 (Mar. 2009), arXiv:0806.2340.
- [104] M. H. Siegel, M. D. Shetrone, and M. Irwin, *Astron. J.* **135**, 2084 (Jun. 2008), arXiv:0803.2489.
- [105] M. Loewenstein and A. Kusenko, *Astrophys. J.* **714**, 652 (May 2010), arXiv:0912.0552 [astro-ph.HE].
- [106] A. Kusenko and M. Loewenstein, *ArXiv e-prints*(Jan. 2010), arXiv:1001.4055 [astro-ph.CO].
- [107] A. Boyarsky, O. Ruchayskiy, D. Iakubovskiy, M. G. Walker, S. Riemer-Sørensen, and S. H. Hansen, *Mon. Not. R. Astron. Soc.* **407**, 1188 (Sep. 2010), arXiv:1001.0644 [astro-ph.CO].
- [108] J. Wolf, G. D. Martinez, J. S. Bullock, M. Kaplinghat, M. Geha, R. R. Munoz, J. D. Simon, and F. F. Avedo, *ArXiv e-prints*(Aug. 2009), arXiv:0908.2995.
- [109] M. Viel, J. Lesgourgues, M. G. Haehnelt, S. Matarrese, and A. Riotto, *Physical Review Letters* **97**, 071301 (Aug. 2006), arXiv:astro-ph/0605706.
- [110] M. Viel, G. D. Becker, J. S. Bolton, M. G. Haehnelt, M. Rauch, and W. L. W. Sargent, *Physical Review Letters* **100**, 041304 (Feb. 2008), arXiv:0709.0131.
- [111] P. McDonald, U. Seljak, S. Burles, D. J. Schlegel, D. H. Weinberg, R. Cen, D. Shih, J. Schaye, D. P. Schneider, N. A. Bahcall, J. W. Briggs, J. Brinkmann, R. J. Brunner, M. Fukugita, J. E. Gunn, Ž. Ivezić, S. Kent, R. H. Lupton, and D. E. Vanden Berk, *Astrophys. J. Suppl.* **163**, 80 (Mar. 2006), arXiv:astro-ph/0405013.
- [112] U. Seljak, A. Makarov, P. McDonald, and H. Trac, *Physical Review Letters* **97**, 191303 (Nov. 2006), arXiv:astro-ph/0602430.
- [113] M. Viel, J. S. Bolton, and M. G. Haehnelt, *Mon. Not. R. Astron. Soc.* **399**, L39 (Oct. 2009), arXiv:0907.2927.
- [114] M. Ricotti, N. Y. Gnedin, and J. M. Shull, *Astrophys. J.* **534**, 41 (May 2000), arXiv:astro-ph/9906413.
- [115] J. Schaye, T. Theuns, M. Rauch, G. Efstathiou, and

- W. L. W. Sargent, *Mon. Not. R. Astron. Soc.* **318**, 817 (Nov. 2000), arXiv:astro-ph/9912432.
- [116] A. Boyarsky, A. Neronov, O. Ruchayskiy, and M. Shaposhnikov, *Mon. Not. R. Astron. Soc.* **370**, 213 (Jul. 2006), arXiv:astro-ph/0512509.
- [117] K. Abazajian and S. M. Koushiappas, *Phys. Rev. D* **74**, 023527 (Jul. 2006), arXiv:astro-ph/0605271.
- [118] A. Boyarsky, A. Neronov, O. Ruchayskiy, and M. Shaposhnikov, *Phys. Rev. D* **74**, 103506 (Nov. 2006), arXiv:astro-ph/0603368.
- [119] S. Riemer-Sørensen, K. Pedersen, S. H. Hansen, and H. Dahle, *Phys. Rev. D* **76**, 043524 (Aug. 2007), arXiv:astro-ph/0610034.
- [120] A. Boyarsky, O. Ruchayskiy, and M. Markevitch, *Astrophys. J.* **673**, 752 (Feb. 2008), arXiv:astro-ph/0611168.
- [121] C. R. Watson, J. F. Beacom, H. Yüksel, and T. P. Walker, *Phys. Rev. D* **74**, 033009 (Aug. 2006), arXiv:astro-ph/0605424.
- [122] A. Boyarsky, J. Nevalainen, and O. Ruchayskiy, *A&A* **471**, 51 (Aug. 2007), arXiv:astro-ph/0610961.
- [123] S. Riemer-Sørensen and S. H. Hansen, *A&A* **500**, L37 (Jun. 2009).
- [124] A. Boyarsky, J. Lesgourgues, O. Ruchayskiy, and M. Viel, *Physical Review Letters* **102**, 201304 (May 2009), arXiv:0812.3256 [hep-ph].
- [125] M. Loewenstein, A. Kusenko, and P. L. Biermann, *Astrophys. J.* **700**, 426 (Jul. 2009), arXiv:0812.2710.
- [126] S. Riemer-Sørensen, S. H. Hansen, and K. Pedersen, *Astrophys. J. Lett.* **644**, L33 (Jun. 2006), arXiv:astro-ph/0603661.
- [127] K. N. Abazajian, M. Markevitch, S. M. Koushiappas, and R. C. Hickox, *Phys. Rev. D* **75**, 063511 (Mar. 2007), arXiv:astro-ph/0611144.
- [128] T. Asaka, M. Shaposhnikov, and A. Kusenko, *Physics Letters B* **638**, 401 (Jul. 2006), arXiv:hep-ph/0602150.

Appendix

We used the BBKS formula for the CDM transfer function when generating the initial conditions for our high resolution simulations. This formula assumes a baryon density of zero. Eisenstein and Hu [32] calculated transfer functions for CDM cosmologies that include baryon physics. We plot the power spectra for the fitting formula of Eisenstein and Hu and the spectrum calculated with the LINGER software (using $\Omega_b = 0.04$) normalized by BBKS in Figure 12. With $\Omega_m = 0.238$ a Milky Way-sized halo with mass $\sim 2 \times 10^{12} M_\odot$ would form from a spherical region with diameter 4.8 Mpc ($k = 0.28 h/\text{Mpc}$); this is plotted along with the scale of the simulation box (90 Mpc) as solid vertical lines. Dashed vertical lines show the cell size in the refinement region of the low and high resolution simulations. Figure 12 shows that, for a fixed value of σ_8 , BBKS underestimates power on scales $k \lesssim 0.1$ but the power spectra are nearly identical for scales $\lesssim 14$ Mpc with BBKS slightly power overabundant by $\sim 10\%$. The *set C* halos showed subhalo abundance variations much greater than 10% and the BBKS power overabundance is much less than the 30% (1σ) intrinsic scatter in subhalo abundance for MW-sized halos that we adopt.

To check if BBKS might affect the number of satellites, we reran the *set B* high resolution CDM using initial conditions generated from the formula of Eisenstein and Hu. The panels of Figure 13 compare the velocity functions of satellites and show good agreement between the simulations and within the scatter of the *set C* simulations. Based on this and the agreement between the BBKS and *set C* simulations seen in Sec. III A, we conclude that the use of BBKS has not introduced a systematic error into our results.

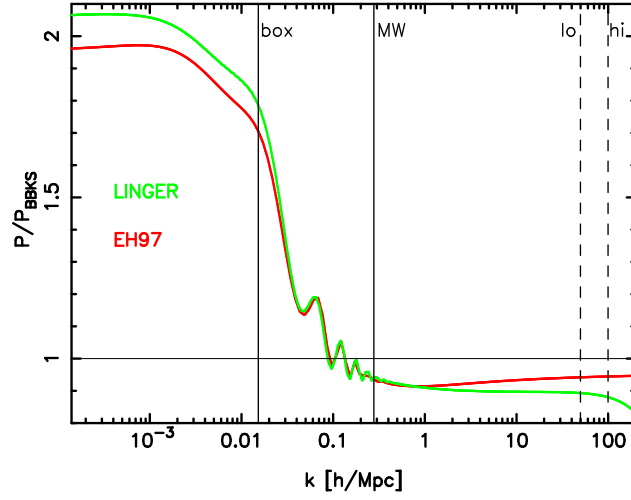


FIG. 12. Comparison of CDM power spectra calculated from the fitting formula of Eisenstein and Hu (EH97) and from the LINGER software normalized by BBKS. On scales $k > 0.1 h/\text{Mpc}$ ($< 14 \text{ Mpc}$) the power spectra are nearly identical. The ‘MW’ vertical line is the diameter of a spherical region with density $\Omega_m \rho_c$ enclosing a Milky Way-sized mass $2 \times 10^{12} M_\odot$ ($\sim 5 \text{ Mpc}$). This scale is well within the range where the power spectra are nearly equal.

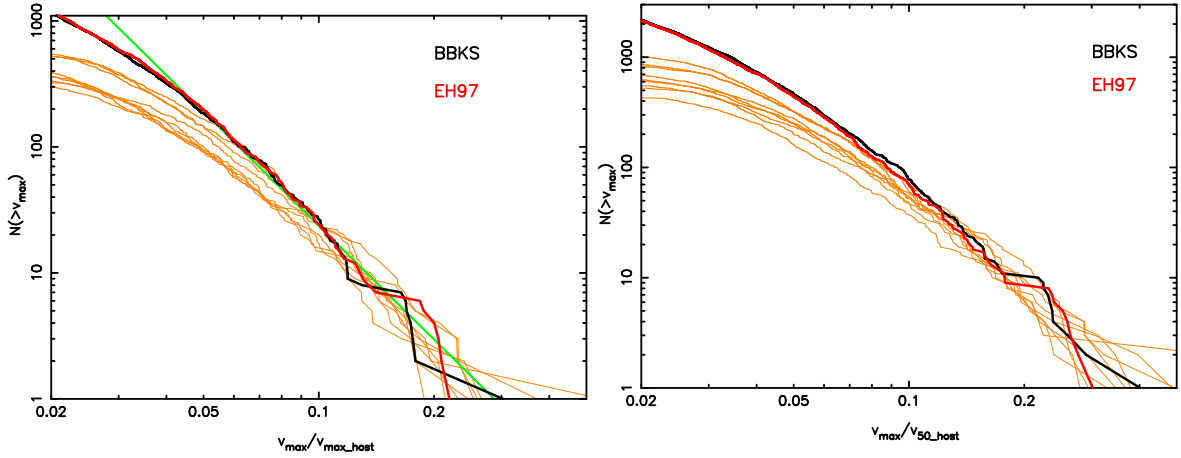


FIG. 13. Subhalo velocity function comparison for CDM high resolution *set B* simulations using fitting formula from BBKS and Eisenstein and Hu (*thick lines*) and the LINGER using *set C* simulations (*thin lines*). (*left*) Subhalos within R_{100} and velocities normalized by v_{max} of their host. The straight sloped line is the fitting formula from the Bolshoi simulation. (*right*) Subhalos within R_{50} , normalized by v_{50} of their host. The subhalo abundances between the BBKS and EH97 simulations are in good agreement and within the scatter of the *set C* halos.